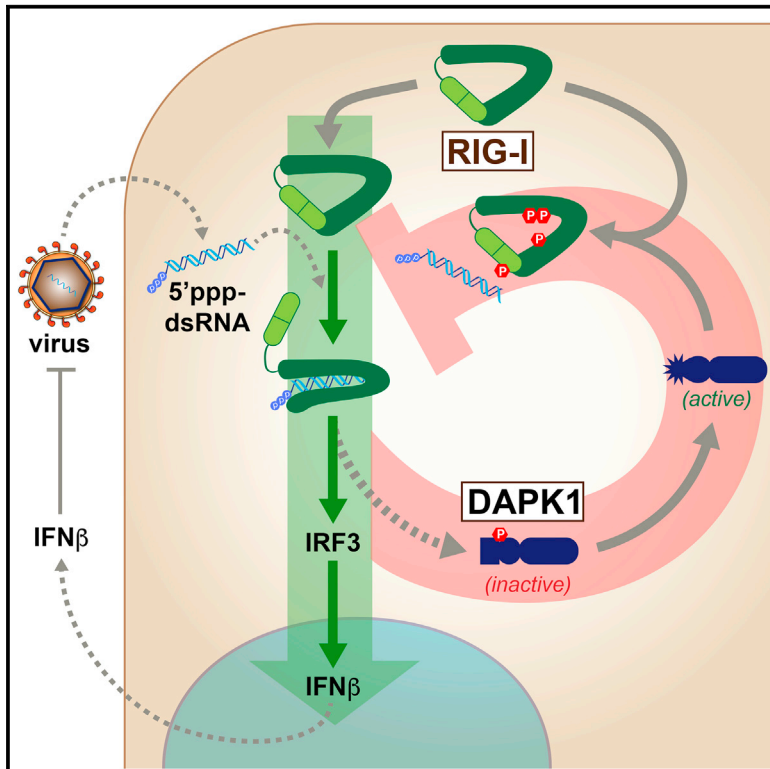


Molecular Cell

Phosphorylation-Dependent Feedback Inhibition of RIG-I by DAPK1 Identified by Kinome-wide siRNA Screening

Graphical Abstract



Authors

Joschka Willemsen, Oliver Wicht, Julia C. Wolanski, ..., Joseph Marcotrigiano, Andreas Pichlmair, Marco Binder

Correspondence

m.binder@dkfz.de

In Brief

Willemsen et al. screened the antiviral RIG-I pathway for regulators and identified and validated 22 kinases. They describe an inhibitory feedback loop mediated by DAPK1. Antiviral signaling activates DAPK1 kinase activity, which, in turn, inactivates RIG-I by direct phosphorylation.

Highlights

- siRNA screen of antiviral RIG-I/IRF3 pathway (human kinome) was performed
- DAPK1 was identified as a negative-feedback regulator of the RIG-I pathway
- RIG-I-mediated antiviral signaling activates DAPK1 kinase activity
- DAPK1 inactivates RIG-I RNA sensing by direct phosphorylation of RIG-I



Phosphorylation-Dependent Feedback Inhibition of RIG-I by DAPK1 Identified by Kinome-wide siRNA Screening

Joschka Willemsen,^{1,2} Oliver Wicht,² Julia C. Wolanski,¹ Nina Baur,² Sandra Bastian,¹ Darya A. Haas,³ Petr Matula,^{4,5} Bettina Knapp,⁶ Laurene Meyniel-Schicklin,⁷ Chen Wang,⁸ Ralf Bartenschlager,⁹ Volker Lohmann,⁹ Karl Rohr,⁴ Holger Erfle,¹⁰ Lars Kaderali,^{6,11} Joseph Marcotrigiano,⁸ Andreas Pichlmair,³ and Marco Binder^{1,2,12,*}

¹Research Group “Dynamics of early viral infection and the innate antiviral response,” Division Virus-associated carcinogenesis (F170), German Cancer Research Center (DKFZ), 69120 Heidelberg, Germany

²Department for Infectious Diseases, Molecular Virology, Research Group “Dynamics of early viral infection and the innate antiviral response,” Medical Faculty, Heidelberg University, 69120 Heidelberg, Germany

³Innate Immunity Laboratory, Max-Planck Institute of Biochemistry, Am Klopferspitz 18, 82152 Martinsried, Germany

⁴Biomedical Computer Vision Group, BioQuant, IPMB, and German Cancer Research Center (DKFZ), Department of Bioinformatics and Functional Genomics, Heidelberg University, 69120 Heidelberg, Germany

⁵Center for Biomedical Image Analysis, Faculty of Informatics, Masaryk University, 60200 Brno, Czech Republic

⁶ViroQuant Research Group Modeling, BioQuant, Heidelberg University, 69120 Heidelberg, Germany

⁷ENYO Pharma, 69007 Lyon, France

⁸Center for Advanced Biotechnology and Medicine, Department of Chemistry and Chemical Biology, Rutgers University, Piscataway, NJ 08854, USA

⁹Department for Infectious Diseases, Molecular Virology, Medical Faculty, Heidelberg University, 69120 Heidelberg, Germany

¹⁰ViroQuant-CellNetworks RNAi Screening Facility, BioQuant, Heidelberg University, 69120 Heidelberg, Germany

¹¹Institute for Bioinformatics, University Medicine Greifswald, 17475 Greifswald, Germany

¹²Lead Contact

*Correspondence: m.binder@dkfz.de

<http://dx.doi.org/10.1016/j.molcel.2016.12.021>

SUMMARY

Cell-autonomous induction of type I interferon must be stringently regulated. Rapid induction is key to control virus infection, whereas proper limitation of signaling is essential to prevent immunopathology and autoimmune disease. Using unbiased kinome-wide RNAi screening followed by thorough validation, we identified 22 factors that regulate RIG-I/IRF3 signaling activity. We describe a negative-feedback mechanism targeting RIG-I activity, which is mediated by death associated protein kinase 1 (DAPK1). RIG-I signaling triggers DAPK1 kinase activation, and active DAPK1 potently inhibits RIG-I stimulated IRF3 activity and interferon-beta production. DAPK1 phosphorylates RIG-I *in vitro* at previously reported as well as other sites that limit 5'ppp-dsRNA sensing and virtually abrogate RIG-I activation.

INTRODUCTION

Detection of invading pathogens by the cells of an organism is key for countering infectious diseases. In vertebrates, virus infection elicits a rapid cell-autonomous immune response initiated by sensing of virus-derived pathogen associated molecular patterns (PAMPs) by germline encoded pattern recognition receptors

(PRRs). The PRRs of the RIG-I-like receptor (RLR) family detect virus derived RNAs. RIG-I (official symbol: DDX58) senses double-stranded RNA (dsRNA) bearing a 5'-triphosphate group (5'ppp-dsRNA), a remnant of the RNA replication process of many RNA viruses. Upon binding to stimulatory RNA, RIG-I undergoes conformational changes allowing it to bind and activate mitochondrial antiviral-signaling protein (MAVS) (Abbas et al., 2013; Binder et al., 2011; Hornung et al., 2006; Patel et al., 2013). Activated RIG-I/MAVS complexes recruit the kinases TBK1 and IKK ϵ , which, in turn, recruit and activate the transcription factor IRF3 (Liu et al., 2015; McNab et al., 2015), as well as the canonical IKKs (α , β , and γ) to activate nuclear factor κ B (NF- κ B). Simultaneous activation of IRF3 and NF- κ B results in the production of type I and type III interferon (IFN), proinflammatory cytokines as well as direct induction of antiviral genes such as IFIT1 (Chan and Gack, 2015). Exposure of cells to IFNs induces expression of a broad panel of IFN stimulated genes (ISGs), which act in concert to protect from virus infections. While this acute response is vital to fight off ubiquitous viruses, overshooting and/or prolonged production of IFNs leads to detrimental side effects, participating in the immunopathology of various infections (Trinchieri, 2010) or even promoting the persistence of virus infection (Teijaro et al., 2013; Wilson et al., 2013). On an organismal level, continuous IFN production is associated with autoimmune disorders (Buers et al., 2016; Crow and Manel, 2015). Therefore, besides swift activation of the IFN system, timely and efficient shut down of the response is equally important (Ivashkiv and Donlin, 2014; Teijaro et al., 2013; Wilson et al., 2013). In contrast to activation of RIG-I signaling, little is known about counter-regulatory mechanisms leading to the termination of signaling.

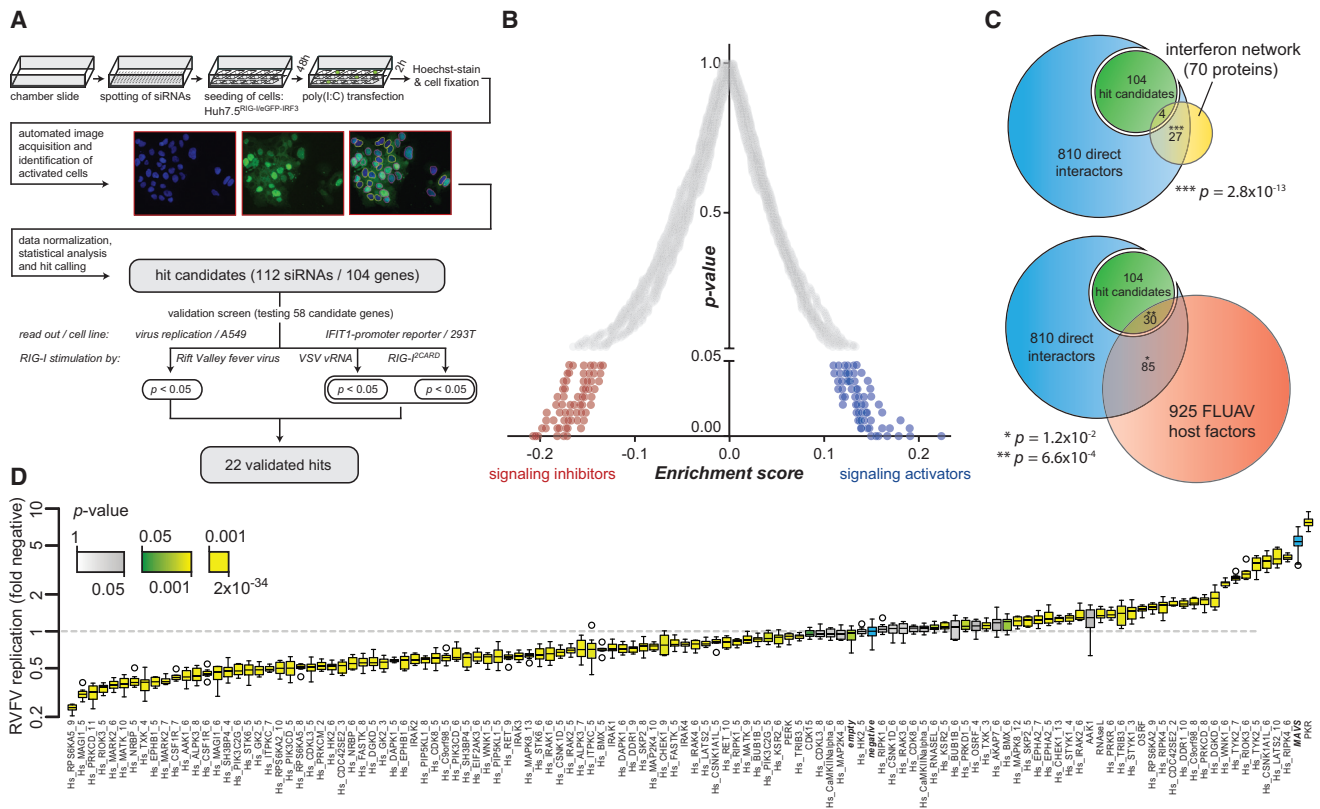


Figure 1. Identification of Kinases that Regulate RIG-I-Mediated IRF3 Translocation

(A) Overview of the screening setup and workflow.

(B) Results of the primary screen, plotting p value over enrichment score for individual siRNAs. SiRNAs against candidate activators (blue) or inhibitors (red) of signaling significantly (p ≤ 0.05) reduced or increased IRF3 translocation, respectively. Data are provided in [Data S1](#).

(C) Venn diagrams demonstrating the overlap of primary hit candidates (green) and their direct protein-protein-interaction (PPI) partners (blue) with the IFN subnetwork in a curated human PPI network (yellow, upper panel) or with published host factors of influenza A virus (FLUAV) replication (red, lower panel). Enrichment p values calculated with Fisher's exact test and indicated in the figure; for PPI maps of hit candidates, see [Figure S1](#).

(D) Validation screening based on Rift Valley fever virus (RVFV): *Renilla* luciferase encoding RVFVΔNSs replication in siRNA-transfected A549^{Ago2} cells; two siRNAs per candidate gene (QIAGEN siRNA ID indicated). Box and whisker plot represents data from nine replicates, with the most extreme replicate (outlier) per siRNA removed. Boxes colored by significance relative to negative control siRNA (t test), color scale given in the figure. For results of other validation screens, see [Figure S2](#).

Constitutive dampening of RIG-I signaling and IFN production has been described recently. For example, activity-promoting ubiquitylation of RIG-I ([Gack et al., 2007](#)) is balanced by deubiquitylation ([Cui et al., 2014](#); [Fan et al., 2014](#)), and activating dephosphorylation of RIG-I by PP1 ([Wies et al., 2013](#)) is countered by inhibitory phosphorylation through PKC ([Maharaj et al., 2012](#)). However, despite clear evidence of negative feedback on RIG-I, very little is known about the identity and regulation of these pathways. Importantly, to allow robust activation of type I IFN production shortly after virus infection, feedback mechanisms aiming at signal termination have to be activated with delayed kinetics. A few recent reports propose negative feedback involving proteasomal targeting of RIG-I ([Arimoto et al., 2008](#); [Kim et al., 2008](#); [Chen et al., 2013](#)). However, given that RIG-I abundance is dramatically upregulated by IFN signaling, degradative mechanisms can only partially explain termination of signaling. Therefore, we hypothesized on the existence of negative-feedback mechanisms that directly affect RIG-I or immediate downstream signaling activity.

Here we used an unbiased kinome-wide RNAi screen to identify positive and negative regulators of RIG-I activation. We validated and characterized 22 genes, most of which have not been reported before to regulate RIG-I signaling. Among these, we identified a previously unknown negative-feedback mechanism that targets RIG-I activity and is mediated by death associated protein kinase 1 (DAPK1).

RESULTS

In order to identify kinases that regulate RIG-I signaling, a kinome-wide small interfering RNA (siRNA) screen was performed in an Huh7.5^{RIG-I}-based cell line ([Binder et al., 2007](#)). Cells were stimulated by transfection of poly(I:C), which specifically triggers RIG-I-dependent signaling in these cells, and activation of antiviral signaling was quantified by assessing nuclear translocation of eGFP-tagged IRF3 ([Figure 1A](#); [STAR Methods](#)). Analysis of primary screening data yielded 104 hit candidates that significantly (p < 0.05) altered IRF3 activation ([Figure 1B](#); [Data S1](#)).

Primary Screening and Bioinformatics

Functional annotation analysis showed strongest enrichment of hit candidates in processes such as cytokinesis, phosphatidylinositol metabolism/signaling, and intracellular protein trafficking but also in disease-associated pathways, TLR signaling, and the innate immune response (Data S2). We further performed network analyses to assess the connectivity of our hit candidates based on a curated human protein-protein-interaction (PPI) network. We found several pairwise interactions between hit candidates, as well as a compact network of 15 interacting hit candidates (Figure S1A). In this network, AKT1 acted as a central hub directly linking to six other candidates, confirming its described role in regulating the induction of the IFN system (Gantner et al., 2012). We further analyzed whether other candidates also directly link to the innate immune IFN network (Navratil et al., 2010). Strikingly, while only four hit candidates were themselves part of the described IFN network (Navratil et al., 2010), we realized that a substantial fraction of candidates (28 out of 104) directly interacted with a highly significant number of proteins ($n = 27$, $p = 3 \times 10^{-13}$) of the IFN system (Figures 1C and S1C; Data S3). This corroborated the quality of the primary screen, identifying genes that have previously not been recognized to be involved in antiviral innate immunity, but that are reasonable due to their close proximity to known members of the IFN response. Lastly, we analyzed our primary candidates for their overlap with published screens for host factors of different viruses. We found a highly significant number of hit candidates (30 out of 104, $p = 7 \times 10^{-4}$) that had been identified as host factors for influenza A virus (FLUAV) (de Chassesey et al., 2012), which is known to be very sensitive to IFN and in particular to the RIG-I pathway (Killip et al., 2015) (Figure 1C; Data S3). This further fostered the notion, that our primary RNAi screen successfully identified genes involved in cellular processes directly or indirectly linked to the innate antiviral response system.

Validation Screening and Hit Characterization

Primary screening identified 104 genes modulating RIG-I/IRF3 signaling. In order to stringently validate hits, the 58 most prominent candidates (based on p value and literature, Data S1) were subjected to three independent rounds of validation screening, employing siRNAs, cell lines, and reporter systems different from the primary screen (see Figures 1A, 2A, and S2). The most robust validation screen (highest Z scores) was based on A549 cells infected with a *Renilla* luciferase encoding Rift Valley fever virus (RVFV Δ NSs Δ RLuc), which is known to very efficiently trigger RIG-I signaling (Kuri et al., 2010). The readout in this setting was the degree of RIG-I/IRF3/IFN-mediated inhibition of RVFV replication (Figure 1D). We considered a hit validated when its effect was significant in the primary, the RVFV and at least one other validation screen (see STAR Methods). Twenty-two genes satisfied these criteria and are therefore considered high-confidence hits reproducibly affecting RIG-I signaling (Figures 2 and S2C; Data S1).

Twenty-one identified hits (AAK1 was excluded for technical reasons) were further characterized with respect to their effect on RIG-I-mediated IRF3 activation upon knockdown or overexpression in 293T^{RIG-I} cells. For the knockdown setting, the respective siRNA yielding the strongest effect in validation

screening was used and IRF3 activity (IFIT1 promoter) luciferase reporter activation as well as endogenous IFIT1 mRNA production were assessed (Figure 2A, upper panel). To complement gene silencing, we further obtained cDNAs for all hit genes and assessed the effect of their overexpression on RIG-I-mediated IRF3 activation. Expression of 16 out of the 21 tested genes lead to dose-dependent modulation of IRF3 activation upon RIG-I stimulation (Figure 2A, lower panel). For several of these genes, the direction of the effect of overexpression was in agreement with the knockdown phenotype (i.e., inverse direction) and also confirmed the phenotype observed in the screens (Figure 2C). Another group of hit genes were “notorious switchers,” i.e., reproducibly showing significant effects in all tested settings but with irreproducible directions. These genes will be challenging but very exciting to follow up on in future studies, as their abundance and/or activity seems to require very fine balancing, which might suggest central roles in the regulatory circuits they are involved in.

In order to establish the relevance of the identified hits within the authentic life cycle of a relevant human pathogen, hit genes were silenced in human lung epithelial A549 cells prior to infection with FLUAV. Staining the viral NP protein and subsequent flow-cytometric analysis demonstrated reproducible and potent effects on the number of FLUAV positive cells for a majority of genes (Figure 2B).

In summary, our high-throughput screen identified 22 genes that reproducibly and significantly affected signaling through the RIG-I pathway, and most of which have not been implicated with innate antiviral signaling before.

Death-Associated Protein Kinase 1 Inhibits RIG-I-Mediated Signaling

Death-Associated Protein Kinase 1 (DAPK1) was one of three genes that stood out by showing significant effects of consistent direction throughout all tested assays (Figure 2C). DAPK1 is a 160-kDa Ca^{2+} -calmodulin (CaM)-dependent serine/threonine kinase, comprised of an N-terminal kinase domain followed by a regulatory CaM binding domain, eight Ankyrin repeats, a cytoskeleton associating ROC-COR domain and a C-terminal death domain (schematic in Figure 4A, interaction network in Figure S1B) (Carlessi et al., 2011). It has been described to be involved in the regulation of a variety of cellular processes such as apoptosis, autophagy, cell motility, and inflammation (Bialik and Kimchi, 2014).

From our screening, DAPK1 was identified as a negative regulator of RIG-I/IRF3 signaling, with its silencing leading to increased transcriptional activity of IRF3, and overexpression leading to a profound decrease (Figure 2A). Accordingly, silencing of DAPK1 had profound negative effects on viral replication, both for RVFV (Figure 1D), as well as for FLUAV (Figure 2B). We further validated this effect on FLUAV by immunofluorescence analysis of infected cells (Figure 3A) and detailed flow cytometry (FACS) analysis (Figure 3B), as well as in virus production assays (Figure 3C), clearly demonstrating a substantial decrease of viral replication in DAPK1-silenced cells.

We then further dissected the inhibitory effect of DAPK1 onto the outcome of RIG-I signaling. In order to discriminate whether

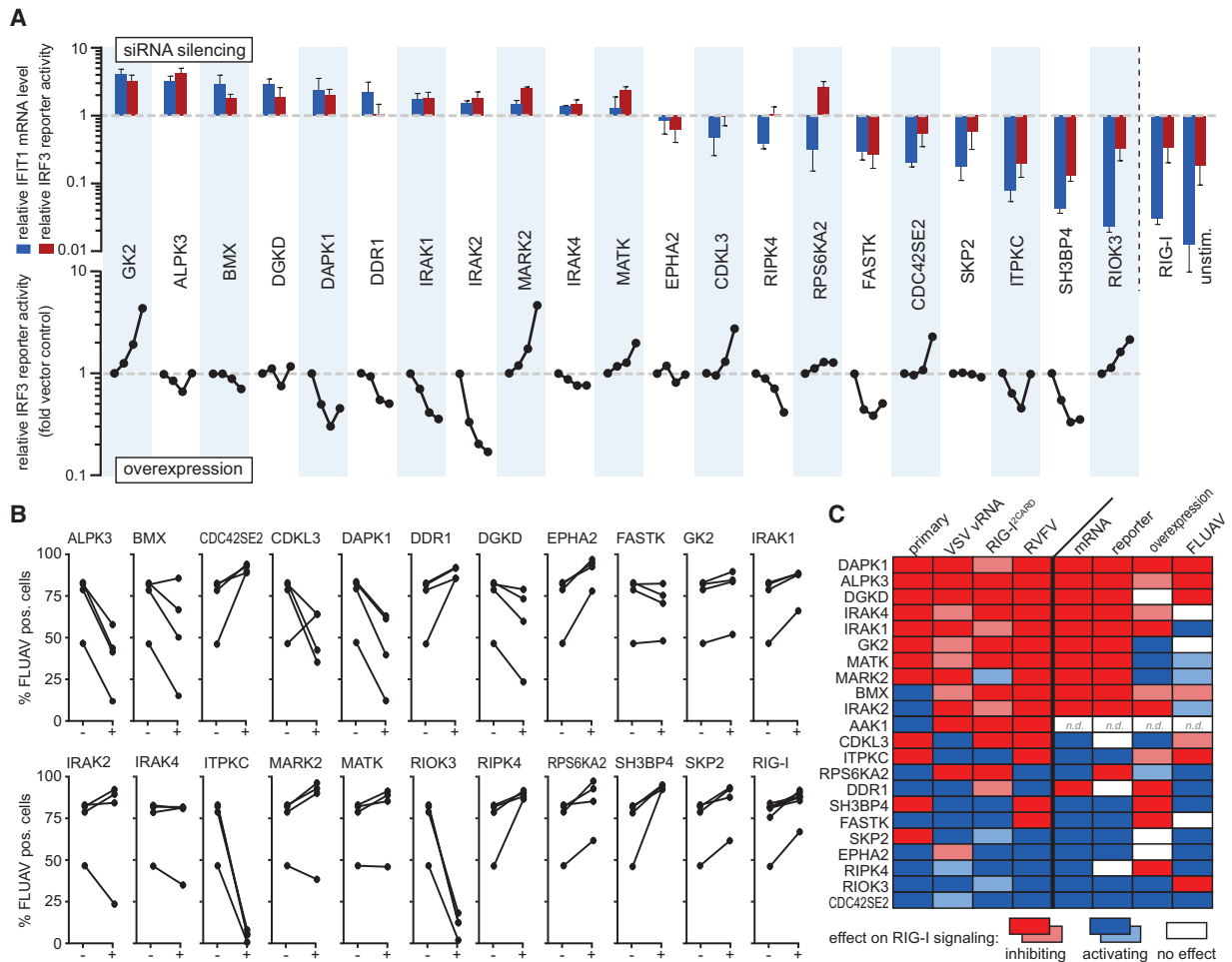


Figure 2. Validation and Characterization of Hit Genes

(A) Validation yielded 22 hit genes (see also Figure S2), which were further characterized. Upper panel: Relative IFIT1 mRNA levels measured by qRT-PCR (blue bars) and IRF3 luciferase reporter activation (red bars) of 293T^{RIG-I} cells transfected with siRNA against the indicated hit gene and stimulated by transfection of poly(I:C). Values represent the mean \pm SEM of three independent experiments. Lower panel: IRF3 luciferase reporter activity in 293T^{RIG-I} cells transfected with increasing amounts of expression constructs (0, 100, 500, 700 ng of plasmid DNA) and subsequently (8 hr post transfection [p.t.]) stimulated by transfection of poly(I:C). Values are means of technical triplicates from one representative out of at least two independent experiments; error bars were omitted for clarity of the figure.

(B) A549 cells were transfected with siRNAs against the indicated hit gene or RIG-I as a positive control and infected with influenza A virus (FLUAV). Virus replication was determined 32 hr post infection (p.i.) by staining of FLUAV NP protein and detection by flow cytometry. Data show four independent experiments, each as a pairwise comparison of negative control siRNA (-) against hit gene targeting siRNA (+).

(C) Matrix of the 22 validated hits and their effects on RIG-I/IRF3 signaling in the indicated assays; clustered according to phenotypes in the screening. Blue, effects of activators of signaling; red, effects of inhibitors of signaling; dark color, strong effect ($p \leq 0.05$ in assays with statistics); light color, marginal effect; white, lack of a discernable effect.

DAPK1 specifically affects activation of either IRF3 or NF- κ B, or whether it regulates the pathway as a whole, we separately analyzed its effects on the activation of IRF3, NF- κ B, and on the expression of IFN- β . Upon silencing, RIG-I-induced NF- κ B activity was increased similarly to IRF3, and accordingly expression of IFN- β mRNA was enhanced (Figure 3D). This effect was reproducible in different human cell lines and in primary mouse lung fibroblasts (Figures S3A–S3C), as well as with different siRNAs (Figures S3C and S3D). Reciprocally, transient overexpression of DAPK1 lead to a dose-dependent inhibition of both IRF3 and NF- κ B activation upon RIG-I stimulation, as well as decreased levels of IFN- β mRNA (Figure 3E). These observations

suggest a role of DAPK1 in regulating RIG-I signaling at the level or upstream of MAVS.

DAPK1 Kinase Activity and Ankyrin Repeats Are Essential for RIG-I Pathway Inhibition

In order to dissect which domains of DAPK1 (Figure 4A) are essential for mediating its inhibitory effect on RIG-I signaling, a series of deletion mutants were tested for their ability to inhibit IRF3 activation. The death domain, the ROC-, and the regulatory CaM-binding domains were dispensable for the inhibitory effect on IRF3 activation. In contrast, a construct lacking both, the Ankyrin repeats and the

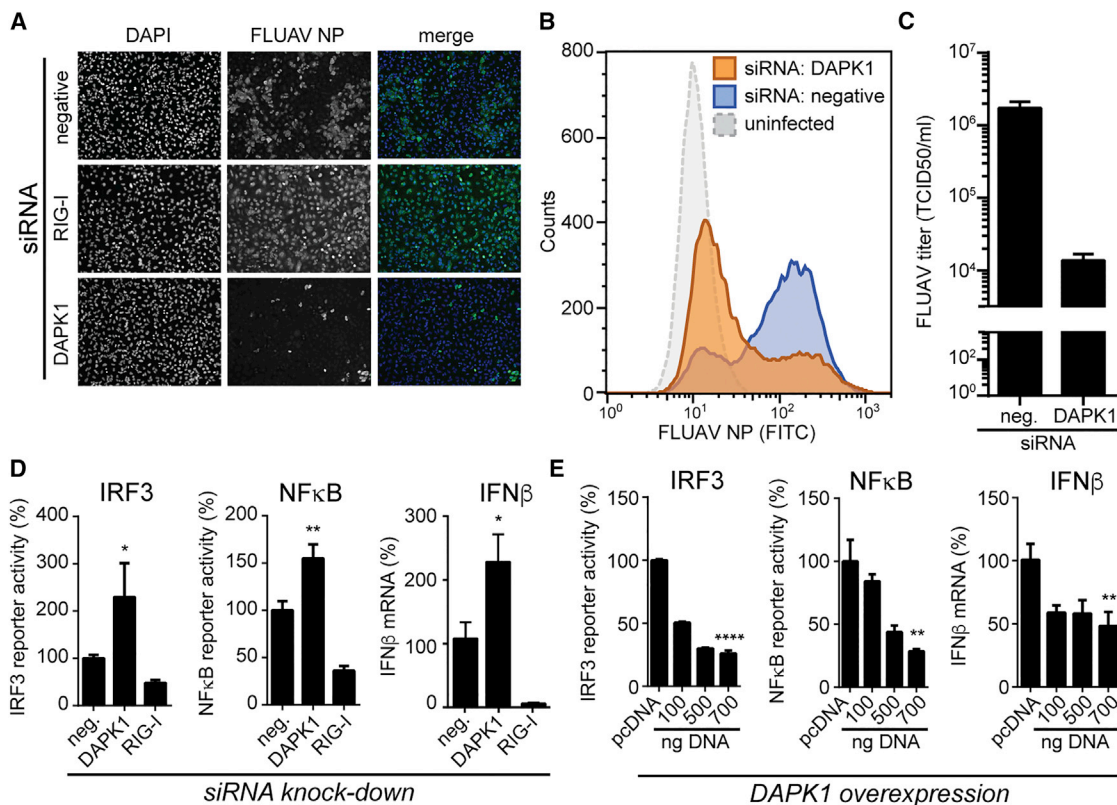


Figure 3. Impact of DAPK1 on Antiviral Signaling

(A–C) A549 cells transfected with the indicated siRNAs were infected with influenza A virus (FLUAV) and infected cells were detected 32 hr p.i. by microscopy (A) or flow cytometry as in Figure 2B. (C) Virus production was measured by TCID₅₀ upon low MOI infection (MOI = 0.001) of A549 cells silenced for DAPK1. Result of one representative out of two independent experiments is shown; error bars represent SD based on replicate wells.

(D) 293T^{RIG-I} cells were transfected with non-targeting siRNA (neg.) or siRNA against DAPK1 or RIG-I as a positive control and stimulated by transfection of poly(I:C). Silencing of DAPK1 lead to increased activity of IRF3 and NF-κB luciferase reporters, as well as to increased expression of IFN-β mRNA. This effect was also confirmed in A549 cells (human) and in primary mouse fibroblasts (Figure S3).

(E) 293T^{RIG-I} cells were transfected with empty vector (pcDNA) or increasing amounts (indicated) of a DAPK1 expression construct and stimulated by transfection of poly(I:C). Overexpression of DAPK1 lead to a dose-dependent inhibition of the activity of IRF3 and NF-κB luciferase reporters, as well as IFN-β mRNA expression. All values represent mean ± SD of technical triplicates from one representative out of three independent experiments. Significance against non-targeting siRNA and empty vector controls, respectively, is denoted with asterisks.

ROC/COR domains, lost its inhibitory potential (Figure 4B), suggesting the Ankyrin repeats domain to be essential for the observed phenotype. Indeed, we could identify a minimal construct comprising only the kinase-, CaM-binding, and Ankyrin repeats domains (Kin|CaM|Ank) to be sufficient to confer the complete inhibition of IRF3 activation (Figure 4C). Neither the Ankyrin repeats nor the kinase domain by themselves were sufficient to inhibit IRF3 activation (Figure 4C). Based on these findings, we hypothesized that the Ankyrin repeats were required for interaction with a potential target, which would then be phosphorylated by the kinase domain. To test whether kinase activity is indeed essential for the down-modulation of RIG-I signaling, we generated enzymatically inactive Kin|CaM|Ank variants. DAPK1 kinase activity has been described to be strictly inhibited by auto-phosphorylation at serine 308 (S308); only upon removal of this phosphate DAPK1 kinase becomes active again (Shohat et al., 2002). We therefore generated phosphomimetic

(S308D) and phosphoablatant (S308A) mutants as described before (Shohat et al., 2001) and tested them for their inhibitory potential on IRF3 activation. Indeed, the constitutively active non-phosphorylatable (S308A) Kin|CaM|Ank variant inhibited RIG-I signaling at least as strongly as wild-type DAPK1, whereas the kinase inactive phosphomimetic (S308D) variant rescued IRF3 activity to a large extent (Figure 4D). Comparable results were obtained with a variant that harbored a 73-aa deletion of the active site, and, to a lesser extent, a variant with a mutated ATP acceptor lysine at position 42 (K42A) (Figure 4D). The lower rescue efficiency of the latter (K42A) likely stems from substantial residual kinase activity of this mutant when expressed in cells (Figure S4B) in contrast to the published in vitro setups (Cohen et al., 1997). These findings support the notion that DAPK1's capacity to inhibit antiviral signaling strongly depends on its Ankyrin repeats domain as well as on the enzymatic activity of its kinase domain.

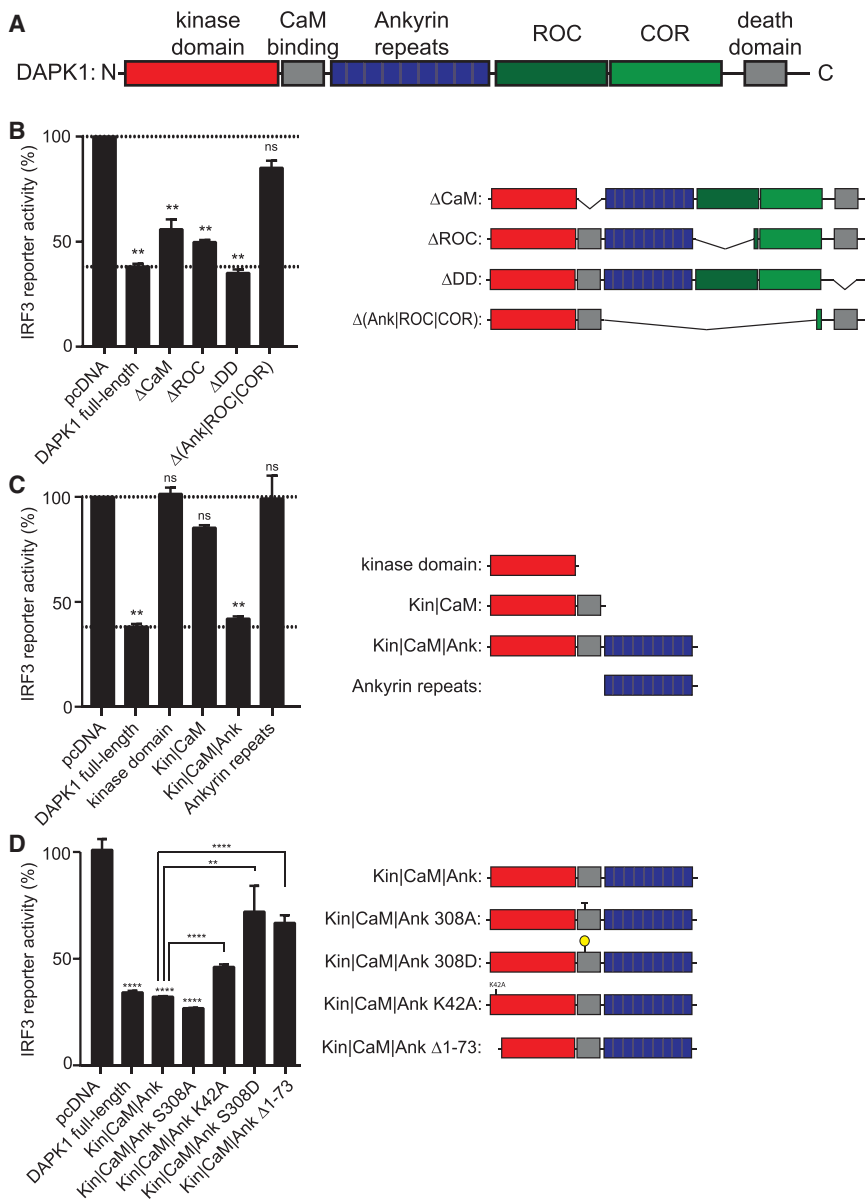


Figure 4. DAPK1 Domains and Activities Required for Inhibition of RIG-I Signaling

(A) Schematic representation of the domain composition of DAPK1.

(B–D) Activity of IRF3 luciferase reporter in 293T^{RIG-I} cells expressing the indicated DAPK1 constructs and stimulated by transfection of poly(I:C). Upper dashed line indicates the IRF3 activation in vector control (pcDNA) cells; lower dashed line indicates IRF3 activation inhibited by expression of full-length DAPK1. Minimal requirement for full inhibition of RIG-I signaling is the kinase domain, CaM binding domain, and Ankyrin repeats (Kin|CaM|Ank) (C) with an active kinase domain (wild-type and S308A) (D). All values represent mean \pm SD of technical triplicates from one representative out of at least three independent experiments. Significance against empty vector controls is denoted with asterisks. See also Figure S4.

phorylation was accompanied by a moderate decrease in total DAPK1 levels, which is in agreement with the reported rapid degradation of activated DAPK1 (Jin et al., 2006). Interestingly, in our kinetic experiments phosphorylation of TBK1 and IRF3, established markers of active RIG-I signaling, increased up to 8- to 12-hr post-stimulation and then started to decrease despite continuously increasing levels of RIG-I (being an ISG). Intriguingly, this pathway deactivation kinetically coincided with the strong activation of DAPK1 after 8 hr (Figure 5B). To confirm that the observed activation of DAPK1 was mediated by antiviral signaling, we performed the same experiment in RIG-I-deficient (CRISPR-KO) A549 cells. In fact, DAPK1 activation was only observed in A549^{WT}, but not in RIG-I-deficient cells (Figure 5C). Further, activation of DAPK1 was independent of

IFN signaling, as exogenous addition of IFN- α did not trigger dephosphorylation of DAPK1 (Figure S5B). This indicated that direct, intracellular signaling events lead to the activation of DAPK1.

Taken together, we concluded that kinase-active DAPK1 is a potent inhibitor of RIG-I/IRF3 signaling, and that DAPK1 itself is activated upon stimulation of RIG-I signaling. This strongly suggested that DAPK1 acts as a negative-feedback regulator of this antiviral signaling pathway. To corroborate this hypothesis, we performed loss-of-function experiments. Upon silencing of DAPK1 by siRNA, stimulation of cells by 5'ppp-dsRNA lead to an increased and prolonged expression of IFIT1 and IFN- β mRNA (Figures 5F and 5G). Importantly, intracellular protein levels of IFN- β closely resembled the kinetics of the mRNA levels (Figure 5, compare panels 5D and 5E to 5G), and also

Stimulation of DAPK1 Kinase Activity upon RIG-I-Mediated Antiviral Signaling

Under physiological conditions, the enzymatic activity of DAPK1 is autoinhibited by default. The most critical step to activate its kinase activity is dephosphorylation of p-S308, which can be triggered by mitochondrial uncoupling, e.g., by treatment of cells with a protonophore such as CCCP (Shang et al., 2005). We tested whether antiviral signaling could activate DAPK1 as well. We therefore assessed activation of endogenous DAPK1 by probing for the phosphorylation status of S308 upon infection of A549 cells with Sendai virus or stimulation by transfection of the RIG-I-specific ligand 5'ppp-dsRNA. Stimulation of RIG-I by virus infection (Figure S5) or 5'ppp-dsRNA substantially decreased the level of S308 phosphorylation over time, comparable to the positive control CCCP (Figures 5A and 5B). Dephos-

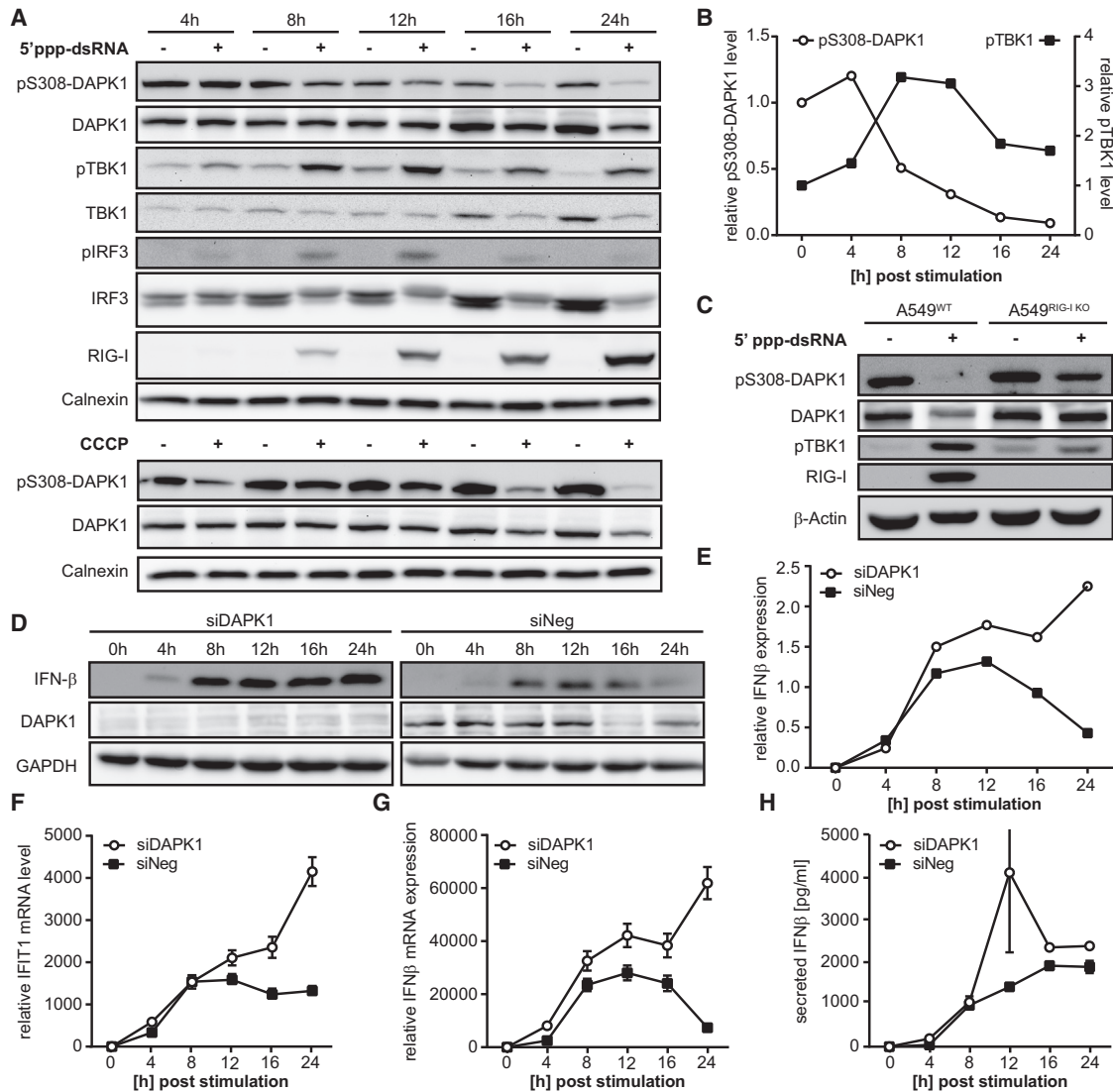


Figure 5. Activation of DAPK1 upon Antiviral Signaling

(A) Immunoblot analysis of A549 cells stimulated by transfection of 5' ppp-dsRNA for the indicated time span (0–24 hr). Signaling through the antiviral RIG-I/IRF3 pathway monitored by detecting phosphorylated TBK1 (pTBK1) and IRF3 (pIRF3) and induction of RIG-I expression (RIG-I is an ISG). RIG-I-signaling-specific activation of DAPK1 was observed by detection of dephosphorylation at serine 308 (pS308) over time. Activation of DAPK1 with the protonophore CCCP served as a positive control (bottom panel). Loading control was calnexin.

(B) Densitometric quantification of immunoblot signals for pS308-DAPK1 and pTBK1 plotted over time post-5' ppp-dsRNA transfection; values are normalized to loading controls and the respective total protein levels of DAPK1 and TBK1. Activation of DAPK1 (= dephosphorylation) precedes deactivation of RIG-I signaling.

(C) Activation of DAPK1 is dependent on active antiviral signaling, as transfection of RIG-I CRISPR/Cas9 knockout cells (A549^{RIG-I KO}) with 5' ppp-dsRNA does not trigger pS308 dephosphorylation.

(D–H) Analysis of mock or DAPK1-silenced (siDAPK1_1) A549 cells stimulated by transfection of 5' ppp-dsRNA for the indicated time span (0–24 hr). IFN-β protein expression was detected by immunoblotting from cell lysates (D and E show densitometric quantification normalized to GAPDH) or by ELISA from cell supernatant (H). IFN-β and IFIT1 mRNA levels were analyzed by qRT-PCR (F) and (G). All data in this figure are showing one representative out of at least two independent experiments (n ≥ 3 for most proteins).

(F–H) Values represent mean ± SD of replicate wells.

See also Figure S5.

secreted levels of IFN-β protein were increased upon DAPK1 silencing (Figure 5H). A repetition (total n = 3) of this experiment is shown in Figures S5C–S5H, in which secretion rates (as opposed to accumulated levels in supernatant) were determined for IFN-β. This observation of increased production

and secretion of IFN-β is very consistent with the observed strong inhibition of virus replication upon DAPK1 silencing (Figure 3). Collectively, these data establish DAPK1 as a potent negative-feedback regulator of the RIG-I antiviral signaling pathway.

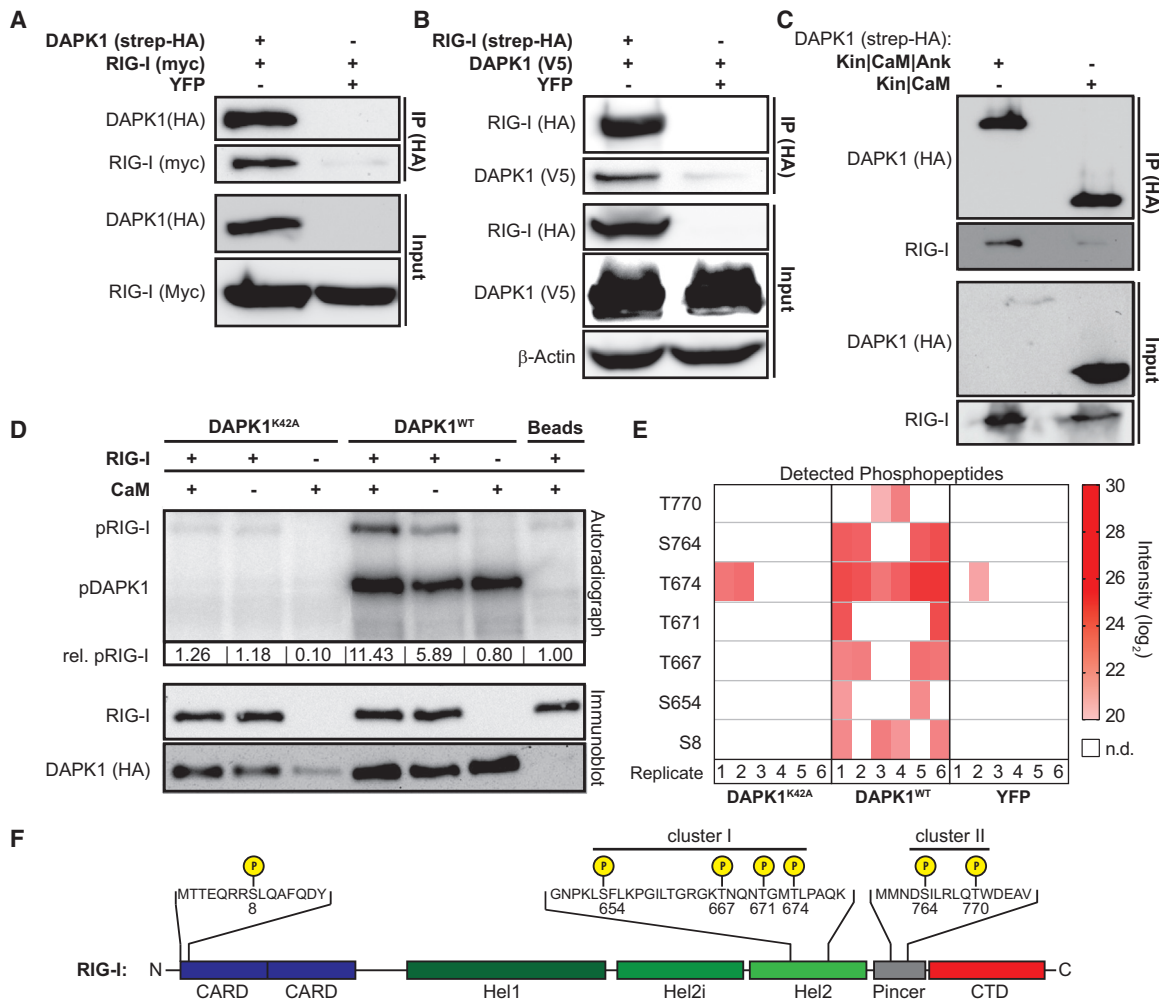


Figure 6. Interaction of DAPK1 with RIG-I

(A and B) Co-immunoprecipitation experiments showed a physical interaction between DAPK1 and RIG-I. 293T cells were transfected with the indicated tagged expression constructs, and either DAPK1 (A) or RIG-I (B) was immunoprecipitated (IP) using an HA-affinity matrix. See also Figure S6.

(C) Truncated variants of DAPK1 (Kin|CaM|Ank and Kin|CaM, see also Figure 4) were expressed in 293T^{RIG-I} cells and immunoprecipitated using an HA-affinity matrix. Only Kin|CaM|Ank interacted significantly with RIG-I.

(D) In vitro γ -³²P-ATP phosphorylation assay using Strep-tag affinity-purified Kin|CaM|Ank of wild-type DAPK1 (DAPK1^{WT}) or enzymatically inactive DAPK1^{K42A} and recombinant RIG-I. Phosphorylation was detected by digital radiography and quantified (relative quantification of phosphorylated RIG-I indicated in panel), amount of proteins was controlled by immunoblotting. A “beads-only” sample (no DAPK1 expressed in cell lysate) was included to control for unspecifically copurifying cellular kinases. Only enzymatically active DAPK1 phosphorylated RIG-I. The blots shown are representative of at least three independent experiments.

(E) Heatmap of DAPK1^{WT}-specific RIG-I phosphorylation sites detected by mass spectrometry from in vitro kinase assays. Measurements were performed in duplicates from three independent in vitro experiments; log₂ intensities are indicated by color.

(F) Identified phosphosites can be clustered in three groups: the very N-terminal S8, cluster I in the Hel2 region, and cluster II in the Pincer domain.

DAPK1 Physically Interacts with and Phosphorylates RIG-I

The simplest interpretation of our findings would be that DAPK1, upon activation, interacts with and phosphorylates a member of the RIG-I-initiated signaling cascade. We therefore screened the most prominent canonical signal transducers of the pathway, namely, RIG-I, MAVS, TRADD, TBK1, IKK ϵ , IRF3, and IRF7 for interaction with DAPK1. Co-precipitation experiments indicated that DAPK1 did not interact with MAVS, TRADD, TBK1, IKK ϵ ,

and IRF3 and only a very weakly and non-reproducibly with IRF7 (Figure S6). Strikingly, however, RIG-I robustly co-precipitated with DAPK1 (Figures 6A, 6B, and S6). Based on our functional findings (Figure 4), we hypothesized that RIG-I would also interact with the minimal Kin|CaM|Ank construct, but not or only weakly with the kinase domain (Kin|CaM). This prediction was confirmed in experiments using these truncated variants of DAPK1 (Figure 6C). Of note, one of the validation screens employed RIG-I^{2CARD} to stimulate signaling and this was the only

assay, in which DAPK1 silencing did not have a significant effect ($p = 0.12$, [Data S1](#)). This also supported the notion of DAPK1 directly targeting RIG-I.

Next, we investigated whether RIG-I might constitute a direct substrate of the DAPK1 kinase. For this purpose, we performed *in vitro* kinase assays using Strep-tag affinity-purified DAPK1^{Kini|CaM|ANK} and recombinant RIG-I in the presence of γ -³²P-ATP. As expected from literature ([Shohat et al., 2001](#)), DAPK1 strongly autophosphorylated itself, but, strikingly, it also robustly phosphorylated RIG-I ([Figure 6D](#)). This phosphorylation was approximately 50% less efficient in the absence of CaM and basically absent in the enzymatically inactive DAPK1^{K42A} control, highlighting the specificity for DAPK1 and ruling out artifacts by potentially co-purifying cellular kinases.

In order to identify the residues in recombinant RIG-I that are phosphorylated by DAPK1, we analyzed *in vitro* phosphorylated RIG-I by mass spectrometry. Seven phosphorylation sites on RIG-I were unambiguously identified in samples containing enzymatically active DAPK1, but not the enzymatically inactive DAPK1^{K42A} variant or an unrelated control protein ([Figure 6E](#)). The identified phosphoserines and phosphothreonines clustered in two distinct regions of the RIG-I protein. Cluster I was located in the Hel2 region of the helicase domain, and cluster II in the pincher domain of RIG-I ([Figure 6F](#)). In addition, we further identified the very N-terminal serine at position 8 (S8) to be phosphorylated by DAPK1. Notably, phosphorylation of this residue by PKC has been reported before to negatively regulate RIG-I activity ([Nistal-Villán et al., 2010](#); [Wies et al., 2013](#)), which is in line with the observed inhibitory effect of DAPK1 onto RIG-I signaling.

Phosphorylation of RIG-I Threonine 667 Impairs 5'ppp-dsRNA Binding and Abolishes Antiviral Signaling

The RIG-I phosphosites in cluster I and II were previously not known. To functionally characterize their effect, we generated phosphomimetic mutants by replacing serines and threonines by glutamic acid or, as a control, by non-phosphorylatable alanines ([Figure S7A](#)). RIG-I mutants were expressed in 293T cells that are virtually devoid of RIG-I, and cells were stimulated by transfection of 5'ppp-dsRNA. As expected, the phosphomimetic of S8 (S8E) significantly reduced IRF3 activation to about 30% of wild-type RIG-I. Mutation of the two residues of cluster II did not affect signaling, but mutation of cluster I completely abolished RIG-I induced IRF3 activation ([Figure 7A](#)). Cluster I resides in the helicase motif IVa of the Hel2 region, which was shown before to be essential for RIG-I signaling ([Devarkar et al., 2016](#)). Upon binding of RIG-I to certain RNAs, such as 5'-OH-hairpinRNA, the motif forms an α -helix and a loop, with cluster I residue T667 residing at the very tip of this loop ([Figure 7B](#)). It was intriguing to speculate that phosphorylation at this prominent position would interfere with RIG-I activation. In line with this hypothesis, phosphomimetic replacement of this single residue by glutamic acid (T667E) sufficed to render RIG-I completely unresponsive to transfected 5'ppp-dsRNA ([Figure 7A](#)). Furthermore, less 5'ppp-dsRNA could be co-precipitated with RIG-I^{T667E} and RIG-I^{T667E/T671E} as compared to RIG-I^{WT} ([Figure 7C](#)). To confirm the strong inhibitory effect of T667 phosphorylation in a more physiological setting, we stably reconstituted A549^{RIG-I KO} cells with RIG-I by lentiviral trans-

duction, either with the wild-type (WT) form or the phosphomimetic variants, and infected these cells with FLUAV. For WT and S8E, we observed robust induction of IFIT1 protein and secretion of IFN λ upon FLUAV infection, whereas phosphomimetics of the cluster I residues, including the individual T667E mutation, almost completely abrogated IFIT1 and IFN λ induction ([Figures 7D](#) and [7E](#)). Accordingly, FLUAV replication was substantially more efficient in cells harboring RIG-I^{T667E} than RIG-I^{WT} as evidenced by FLUAV-NP-specific FACS analysis ([Figure 7F](#)).

Together, these findings offer a sound explanation for the strong inhibitory effect of enzymatically active DAPK1 on RIG-I pathway activity. In light of the observed activation of DAPK1 upon antiviral signaling and the increased and prolonged production of IFN- β upon knockdown of DAPK1, these data strongly support a model wherein DAPK1, by phosphorylation of RIG-I, acts as a negative-feedback regulator of RIG-I/IRF3 signaling, involved in the timely downregulation of antiviral signaling and the re-establishment of cellular homeostasis.

DISCUSSION

We have performed an unbiased screen across all annotated human kinases for regulators of antiviral RIG-I signaling and identified 104 genes significantly modulating IRF3 activation upon stimulation of RIG-I by dsRNA. Two elegant studies have been published screening genome-wide for factors regulating RLR signaling, one from the Krishnan lab ([Pulloor et al., 2014](#)) and one from the Lamarre lab ([Baril et al., 2013](#)). The Krishnan screen revealed a functionally important role of inositol pyrophosphates in the induction of type I IFN. While our screen did not identify (or not cover) the same genes as theirs, functional annotation clustering did reveal a strong enrichment of candidate genes in phosphatidylinositol and inositolphosphate metabolism and signaling, including PI3K enzymes and ITPKC ([Data S2](#), cluster 2). The screen by Lamarre identified Wnt/ β -catenin signaling as an inhibitory system for RLR signaling and IFN- β induction. In line with their model, in our primary screen we found significant effects for isoforms of canonical downstream kinases of Wnt-signaling, such as GSK3 α and GSK3 β or the CSNK1A1 paralog CSNK1G2 and the closely related CSNK1A1L. Moreover, our screen identified AKT1, which can also directly activate β -catenin ([Fang et al., 2007](#); [Luo et al., 2015](#)), and several interacting proteins ([Figure S1A](#)). The observation that the two published studies and ours, despite different technical setups and siRNA libraries, identify similar pathways, underscores the quality and biological relevance of the three screens. It further highlights the general importance to compare high-throughput data on a functional or pathway level, rather than on the level of individual genes.

Our primary screen did not identify canonical antiviral signal transducers, such as IKK ϵ or TBK1, which might be due to inherent redundancy of these kinases. Instead, it identified genes from different cellular pathways and functional modules that are directly or indirectly linked to the antiviral response, which was also highlighted by PPI network analyses and functional annotation clustering. One such functional module is glucose metabolism ([Data S2](#), cluster 17): out of four kinase

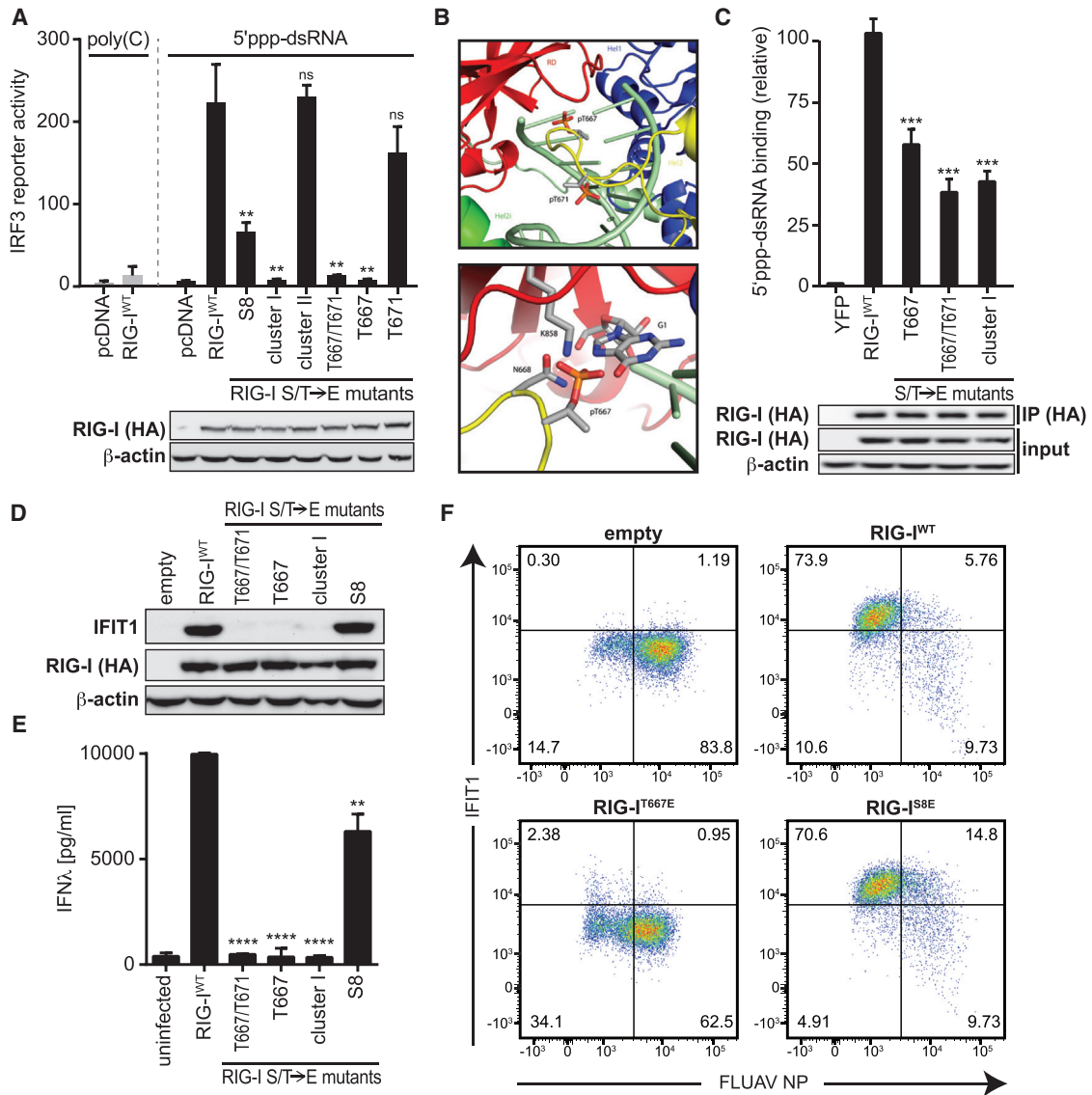


Figure 7. Impact of RIG-I Phosphorylation on the Mounting of an Antiviral Response

(A) IRF3 luciferase reporter activation in 293T cells transfected with empty vector (pcDNA), wild-type RIG-I (RIG-I^{WT}), or the indicated phosphomimetic mutants of RIG-I and stimulation by transfection of 5' ppp-dsRNA. Expression was controlled by immunoblotting (lower panel). Mimicking of phosphorylation at T667 virtually completely abrogates RIG-I signaling.

(B) Phosphorylation of threonine 667 modeled into the crystal structure of 5'-OH-dsRNA-bound RIG-I (PDBID 5F9F). T667 resides at the tip of a conditional loop structure in motif IVa of the Hel2 region and is in close proximity to the terminus of the bound dsRNA.

(C) Immunoprecipitation of RIG-I^{WT} or the indicated phosphomimetic mutants (S/T → E) from 293T cells transfected with 5' ppp-dsRNA. Co-precipitated RNA was measured by qRT-PCR and RIG-I levels were controlled for by immunoblotting. Phosphorylation of the cluster I sites prevents dsRNA binding.

(D–F) IFIT1 immunoblotting (D), IFN-λ ELISA (E), and flow-cytometric analysis (F) of A549^{RIG-I KO} (CRISPR/Cas9 knockout) cells reconstituted with RIG-I^{WT} or the indicated phosphomimetic mutant and infected with FLUAV. Phosphorylation of cluster I sites abrogates IFN production and ISG expression and promotes FLUAV replication. Data are from one representative out of three independent experiments.

(A, C, and E) Data show mean ± SD of technical replicates in one representative out of three independent experiments. Significance against RIG-I^{WT} sample is denoted with asterisks.

See also Figure S7.

activities required for core glycolysis, isoforms of three were identified as hit candidates in our screen (HK2, PKLR, and PFKL). This is particularly interesting in the light of mounting evidence for a major functional crosstalk between metabolism and

various aspects of immunity (Haneklaus and O'Neill, 2015; Wolf et al., 2016).

In three independent rounds of secondary screening, 22 hits could be validated. Twenty-one of them were further studied in

a variety of different assays, providing a rich source of functional data. Ongoing and future studies can build upon these data and are likely to reveal exciting insight into the regulation of innate immunity and its interplay with other cellular processes.

DAPK1 was picked for further in depth characterization as it showed a very robust and interesting phenotype in our assays: (1) ectopic expression of DAPK1 leads to profound and dose-dependent inhibition of RIG-I-mediated IRF3 and NF- κ B activity as well as IFN- β expression; (2) silencing of the gene promotes these activities; (3) silencing of DAPK1 boosts IFN- β production and substantially suppresses replication of two unrelated viruses, RVFV and FLUAV. Together, these findings establish DAPK1 as an inhibitor of RIG-I signaling. An involvement of DAPK1 in antiviral responses has only recently been described by one study, which, in the contrary to our present work, found DAPK1 to promote IRF3 and IRF7 activation and IFN- β production (Zhang et al., 2014). The reason for the contradictory findings remains enigmatic; so far, we were not able to obtain the cells and reagents from the authors and, hence, cannot rule out cell-type-specific differences between their 293 cells and the four different human (Huh-7, 293T, A549) and murine (primary fibroblasts) cell types used in our study. Possibly, a second, independent effect of DAPK1 at the level of the IRFs is dominant in their cell system. This would also be compatible with their observation of the effect's being independent of DAPK1 kinase-activity, which, again, is in stark contrast to our findings.

We found that the active kinase domain in conjunction with the Ankyrin repeats of DAPK1 are required and sufficient to mediate inhibition of RIG-I signaling. This argues for a classical phosphorylation dependent regulation of the RIG-I pathway upon activation of DAPK1. It has been described, that DAPK1 gets activated upon mitochondrial depolarization (Shang et al., 2005). Indeed, treatment of cells with the protonophore CCCP leads to activation of DAPK1 and to a decrease in RIG-I stimulated IRF3 activation (data not shown). This could, however, also be due to indirect effects, as mitochondrial integrity has been shown to be essential for MAVS signaling (Jacobs and Coyne, 2013; Koshiba et al., 2011). Very interesting, though, is our observation that DAPK1 becomes activated upon RIG-I dependent triggering of antiviral signaling. Strikingly, the kinetics of DAPK1 activation shortly precedes the deactivation of RIG-I signaling. Knowing that dephosphorylated (= activated) DAPK1 potently inhibits RIG-I signaling, this finding strongly suggests that the kinase constitutes a negative-feedback regulator of antiviral signaling.

Screening for direct interactors of DAPK1 within the antiviral signaling cascade, we could, in contrast to the study by Zhang et al. (2014), not find robust interaction with IRF3 or IRF7. Instead, we found that DAPK1 interacts with the PAMP sensor RIG-I. This interaction is rather weak and can only be reliably shown in overexpression conditions. Nevertheless, interactions of kinases with their substrates are notoriously weak and extremely transient; hence, the identified interaction is very likely meaningful. By biochemical *in vitro* phosphorylation assays, we demonstrated that RIG-I in fact is a substrate of DAPK1 and becomes phosphorylated at a number of serine and threonine residues. In line with our model of kinase activity-dependent inhibition of RIG-I, one of these residues was serine 8, phosphorylation of which by PKC α and β has been described before to

negatively regulate RIG-I activation (Nistal-Villán et al., 2010; Wies et al., 2013). It is intriguing to speculate that S8 phosphorylation status and corresponding RIG-I signaling competence is regulated by the dynamic equilibrium between (possibly constitutive) phosphorylation by PKC, dephosphorylation by PP1 (Wies et al., 2013) and feedback-induced phosphorylation by DAPK1. Strikingly, however, we identified another, previously undescribed residue in RIG-I that is phosphorylated by DAPK1 and shows a substantially larger effect: a phosphomimetic of threonine at position 667 (T667E) virtually completely abrogates RIG-I signaling in response to 5'ppp-dsRNA, whereas the non-phosphorylatable mutation T667A is almost as effectively signaling as the wild-type. T667 resides in motif IVa of the helicase domain, a highly interesting motif that is intrinsically disordered in the unbound protein (Luo et al., 2011), thereby representing an ideal kinase substrate (Iakoucheva et al., 2004). It was shown previously that upon binding to 5'-OH- but not to 5'ppp-hairpinRNA, this motif forms into a loop- α -helix conformation (Devarkar et al., 2016), in which T667 marks the tip of the loop structure protruding furthest toward the terminus of the bound RNA. Presence of a phosphoryl-threonine at position 667 might stabilize this structure by electrostatic interaction with a basic residue in the regulatory domain (K858, Figure 7B). It therefore is intriguing to speculate that phosphorylation or phosphomimetic mutation of T667 might impact RNA binding, and our RNA-co-precipitation experiments also hint toward this possibility. However, more meaningful equilibrium based biochemical assays will be required to definitely answer this question.

Taken together, our kinome-wide RNAi screening approach identified 22 genes modulating antiviral signaling through the RIG-I/IRF3 axis. One of these genes, DAPK1, could be established as a potent negative-feedback regulator that is activated upon virus infection and antiviral signaling. Subsequently, it leads to downregulation of the signal generated by RIG-I by means of inhibitory phosphorylation of the sensor at residues including the previously described S8 and the here-identified T667. Phosphorylation of T667 almost completely abrogates RIG-I signaling in response to 5'ppp-dsRNA, which is the major ligand for this receptor during virus infection. Accordingly, knockdown of the feedback regulator DAPK1 leads to a profound inhibition of replication of the human pathogens RVFV and FLUAV, whereas mimicking constitutive phosphorylation of RIG-I by DAPK1 results in a drastic increase of FLUAV replication. The impact of this study will be manifold, ranging from a better insight into the physiological termination of antiviral inflammatory signaling, improving the structural understanding of ligand binding and activation of RIG-I, to improving the design of novel synthetic agonists and antagonists of RIG-I for clinical use.

STAR★METHODS

Detailed methods are provided in the online version of this paper and include the following:

- KEY RESOURCES TABLE
- CONTACT FOR REAGENT AND RESOURCE SHARING

- **EXPERIMENTAL MODEL AND SUBJECT DETAILS**

- Cell lines
- Primary cells
- Viruses

- **METHOD DETAILS**

- Cells and cell culture
- siRNA screening
- Cloning and plasmids
- Gene silencing by siRNA
- Overexpression of hit genes
- RIG-I signaling assays
- RIG-I pathway probing with influenza virus
- Immunoblotting
- Immunoprecipitation
- RNA immunoprecipitation
- RIG-I phosphorylation assays

- **QUANTIFICATION AND STATISTICAL ANALYSIS**

- Analysis of primary siRNA screen
- Analysis of secondary siRNA screens
- Quantitative immunoblot analysis
- Analysis of mass-spectrometry data
- General statistical testing

- **DATA AND SOFTWARE AVAILABILITY**

SUPPLEMENTAL INFORMATION

Supplemental Information includes seven figures, four tables, and three data files and can be found with this article online at <http://dx.doi.org/10.1016/j.molcel.2016.12.021>.

AUTHOR CONTRIBUTIONS

The study was conceived and designed and the paper written by M.B. and J.W.; experiments were performed by J.W., O.W., J.C.W., N.B., S.B., D.A.H., and M.B.; data were analyzed by J.W., D.A.H., P.M., B.K., L.M.-S., C.W., L.K., J.M., A.P., and M.B.; reagents and/or technical infrastructure and/or intellectual input indispensable for the study was/were provided by R.B., V.L., K.R., and H.E.

ACKNOWLEDGMENTS

We thank C. Hüber, I. Aydin, S. Rupp, and J. Frankish for their work that regrettably did not make it into the manuscript. Work was supported by DFG BI1693/1-1 (to M.B.), the Medical Faculty Heidelberg Postdoc Fellowship (to M.B.), DFG TRR179 (to M.B., R.B., V.L., and A.P.), BMBF eBio ImmunoQuant (to M.B., R.B., K.R., H.E., and L.K.), GBP302/12/G157 (to P.M.), BMBF FORSYS ViroQuant (to P.M., R.B., V.L., K.R., H.E., and L.K.), and EU FP7 SysPatho (to R.B. and L.K.). The ViroQuant-CellNetworks RNAi screening core facility is supported by CellNetworks - Cluster of Excellence (EXC81).

Received: September 6, 2016

Revised: September 28, 2016

Accepted: December 20, 2016

Published: January 26, 2017

REFERENCES

Abbas, Y.M., Pichlmair, A., Gónna, M.W., Superti-Furga, G., and Nagar, B. (2013). Structural basis for viral 5'-PPP-RNA recognition by human IFIT proteins. *Nature* *494*, 60–64.

Arimoto, K., Konishi, H., and Shimotohno, K. (2008). UbcH8 regulates ubiquitin and ISG15 conjugation to RIG-I. *Mol. Immunol.* *45*, 1078–1084.

Baril, M., Es-Saad, S., Chatel-Chaix, L., Fink, K., Pham, T., Raymond, V.A., Audette, K., Guenier, A.S., Duchaine, J., Servant, M., et al. (2013). Genome-wide RNAi screen reveals a new role of a WNT/CTNBB1 signaling pathway as negative regulator of virus-induced innate immune responses. *PLoS Pathog.* *9*, e1003416.

Bialik, S., and Kimchi, A. (2014). The DAP-kinase interactome. *Apoptosis* *19*, 316–328.

Binder, M., Kochs, G., Bartenschlager, R., and Lohmann, V. (2007). Hepatitis C virus escape from the interferon regulatory factor 3 pathway by a passive and active evasion strategy. *Hepatology* *46*, 1365–1374.

Binder, M., Eberle, F., Seitz, S., Mücke, N., Hüber, C.M., Kiani, N., Kaderali, L., Lohmann, V., Dalpke, A., and Bartenschlager, R. (2011). Molecular mechanism of signal perception and integration by the innate immune sensor retinoic acid-inducible gene-I (RIG-I). *J. Biol. Chem.* *286*, 27278–27287.

Börner, K., Niopek, D., Cotugno, G., Kaldenbach, M., Pankert, T., Willemsen, J., Zhang, X., Schürmann, N., Mockenhaupt, S., Serva, A., et al. (2013). Robust RNAi enhancement via human Argonaute-2 overexpression from plasmids, viral vectors and cell lines. *Nucleic Acids Res.* *41*, e199.

Buers, I., Nitschke, Y., and Rutsch, F. (2016). Novel interferonopathies associated with mutations in RIG-I like receptors. *Cytokine Growth Factor Rev.* *29*, 101–107.

Carlessi, R., Levin-Salomon, V., Ciprut, S., Bialik, S., Berissi, H., Albeck, S., Peleg, Y., and Kimchi, A. (2011). GTP binding to the ROC domain of DAP-kinase regulates its function through intramolecular signalling. *EMBO Rep.* *12*, 917–923.

Chan, Y.K., and Gack, M.U. (2015). RIG-I-like receptor regulation in virus infection and immunity. *Curr. Opin. Virol.* *12*, 7–14.

Chen, W., Han, C., Xie, B., Hu, X., Yu, Q., Shi, L., Wang, Q., Li, D., Wang, J., Zheng, P., et al. (2013). Induction of Siglec-G by RNA viruses inhibits the innate immune response by promoting RIG-I degradation. *Cell* *152*, 467–478.

Cohen, O., Feinstein, E., and Kimchi, A. (1997). DAP-kinase is a Ca²⁺/calmodulin-dependent, cytoskeletal-associated protein kinase, with cell death-inducing functions that depend on its catalytic activity. *EMBO J.* *16*, 998–1008.

Cox, J., and Mann, M. (2008). MaxQuant enables high peptide identification rates, individualized p.p.b.-range mass accuracies and proteome-wide protein quantification. *Nat. Biotechnol.* *26*, 1367–1372.

Cox, J., Michalski, A., and Mann, M. (2011). Software lock mass by two-dimensional minimization of peptide mass errors. *J. Am. Soc. Mass Spectrom.* *22*, 1373–1380.

Crow, Y.J., and Manel, N. (2015). Aicardi-Goutières syndrome and the type I interferonopathies. *Nat. Rev. Immunol.* *15*, 429–440.

Cui, J., Song, Y., Li, Y., Zhu, Q., Tan, P., Qin, Y., Wang, H.Y., and Wang, R.F. (2014). USP3 inhibits type I interferon signaling by deubiquitinating RIG-I-like receptors. *Cell Res.* *24*, 400–416.

de Chasse, B., Meyniel-Schicklin, L., Aublin-Gex, A., André, P., and Lotteau, V. (2012). Genetic screens for the control of influenza virus replication: From meta-analysis to drug discovery. *Mol. Biosyst.* *8*, 1297–1303.

Devarkar, S.C., Wang, C., Miller, M.T., Ramanathan, A., Jiang, F., Khan, A.G., Patel, S.S., and Marcotrigiano, J. (2016). Structural basis for m7G recognition and 2'-O-methyl discrimination in capped RNAs by the innate immune receptor RIG-I. *Proc. Natl. Acad. Sci. USA* *113*, 596–601.

Erfle, H., Neumann, B., Liebel, U., Rogers, P., Held, M., Walter, T., Ellenberg, J., and Pepperkok, R. (2007). Reverse transfection on cell arrays for high content screening microscopy. *Nat. Protoc.* *2*, 392–399.

Fan, Y., Mao, R., Yu, Y., Liu, S., Shi, Z., Cheng, J., Zhang, H., An, L., Zhao, Y., Xu, X., et al. (2014). USP21 negatively regulates antiviral response by acting as a RIG-I deubiquitinase. *J. Exp. Med.* *211*, 313–328.

Fang, D., Hawke, D., Zheng, Y., Xia, Y., Meisenhelder, J., Nika, H., Mills, G.B., Kobayashi, R., Hunter, T., and Lu, Z. (2007). Phosphorylation of beta-catenin by AKT promotes beta-catenin transcriptional activity. *J. Biol. Chem.* *282*, 11221–11229.

Gack, M.U., Shin, Y.C., Joo, C.H., Urano, T., Liang, C., Sun, L., Takeuchi, O., Akira, S., Chen, Z., Inoue, S., and Jung, J.U. (2007). TRIM25 RING-finger E3 ubiquitin ligase is essential for RIG-I-mediated antiviral activity. *Nature* *446*, 916–920.

- Gantner, B.N., Jin, H., Qian, F., Hay, N., He, B., and Ye, R.D. (2012). The Akt1 isoform is required for optimal IFN- β transcription through direct phosphorylation of β -catenin. *J. Immunol.* *189*, 3104–3111.
- Habjan, M., Hubel, P., Lacerda, L., Benda, C., Holze, C., Eberl, C.H., Mann, A., Kindler, E., Gil-Cruz, C., Ziebuhr, J., et al. (2013). Sequestration by IFIT1 impairs translation of 2'-O-unmethylated capped RNA. *PLoS Pathog.* *9*, e1003663.
- Haneklaus, M., and O'Neill, L.A. (2015). NLRP3 at the interface of metabolism and inflammation. *Immunol. Rev.* *265*, 53–62.
- Hornung, V., Ellegast, J., Kim, S., Brzózka, K., Jung, A., Kato, H., Poeck, H., Akira, S., Conzelmann, K.K., Schlee, M., et al. (2006). 5'-Triphosphate RNA is the ligand for RIG-I. *Science* *314*, 994–997.
- Huang, W., Sherman, B.T., and Lempicki, R.A. (2009a). Bioinformatics enrichment tools: Paths toward the comprehensive functional analysis of large gene lists. *Nucleic Acids Res.* *37*, 1–13.
- Huang, W., Sherman, B.T., and Lempicki, R.A. (2009b). Systematic and integrative analysis of large gene lists using DAVID bioinformatics resources. *Nat. Protoc.* *4*, 44–57.
- Iakoucheva, L.M., Radivojac, P., Brown, C.J., O'Connor, T.R., Sikes, J.G., Obradovic, Z., and Dunker, A.K. (2004). The importance of intrinsic disorder for protein phosphorylation. *Nucleic Acids Res.* *32*, 1037–1049.
- Ivashkiv, L.B., and Donlin, L.T. (2014). Regulation of type I interferon responses. *Nat. Rev. Immunol.* *14*, 36–49.
- Jacobs, J.L., and Coyne, C.B. (2013). Mechanisms of MAVS regulation at the mitochondrial membrane. *J. Mol. Biol.* *425*, 5009–5019.
- Jiang, F., Ramanathan, A., Miller, M.T., Tang, G.Q., Gale, M., Jr., Patel, S.S., and Marcotrigiano, J. (2011). Structural basis of RNA recognition and activation by innate immune receptor RIG-I. *Nature* *479*, 423–427.
- Jin, Y., Blue, E.K., and Gallagher, P.J. (2006). Control of death-associated protein kinase (DAPK) activity by phosphorylation and proteasomal degradation. *J. Biol. Chem.* *281*, 39033–39040.
- Killip, M.J., Fodor, E., and Randall, R.E. (2015). Influenza virus activation of the interferon system. *Virus Res.* *209*, 11–22.
- Kim, M.J., Hwang, S.Y., Imaizumi, T., and Yoo, J.Y. (2008). Negative feedback regulation of RIG-I-mediated antiviral signaling by interferon-induced ISG15 conjugation. *J. Virol.* *82*, 1474–1483.
- Knapp, B., Rebhan, I., Kumar, A., Matula, P., Kiani, N.A., Binder, M., Erfle, H., Rohr, K., Eils, R., Bartenschlager, R., and Kaderali, L. (2011). Normalizing for individual cell population context in the analysis of high-content cellular screens. *BMC Bioinformatics* *12*, 485.
- Koshiba, T., Yasukawa, K., Yanagi, Y., and Kawabata, S. (2011). Mitochondrial membrane potential is required for MAVS-mediated antiviral signaling. *Sci. Signal.* *4*, ra7.
- Kuri, T., Habjan, M., Penski, N., and Weber, F. (2010). Species-independent bioassay for sensitive quantification of antiviral type I interferons. *Virol. J.* *7*, 50.
- Liu, S., Cai, X., Wu, J., Cong, Q., Chen, X., Li, T., Du, F., Ren, J., Wu, Y.T., Grishin, N.V., and Chen, Z.J. (2015). Phosphorylation of innate immune adaptor proteins MAVS, STING, and TRIF induces IRF3 activation. *Science* *347*, aaa2630.
- Luo, D., Ding, S.C., Vela, A., Kohlway, A., Lindenbach, B.D., and Pyle, A.M. (2011). Structural insights into RNA recognition by RIG-I. *Cell* *147*, 409–422.
- Luo, W., Zhao, X., Jin, H., Tao, L., Zhu, J., Wang, H., Hemmings, B.A., and Yang, Z. (2015). Akt1 signaling coordinates BMP signaling and β -catenin activity to regulate second heart field progenitor development. *Development* *142*, 732–742.
- Maharaj, N.P., Wies, E., Stoll, A., and Gack, M.U. (2012). Conventional protein kinase C- α (PKC- α) and PKC- β negatively regulate RIG-I antiviral signal transduction. *J. Virol.* *86*, 1358–1371.
- Matula, P., Kumar, A., Wörz, I., Erfle, H., Bartenschlager, R., Eils, R., and Rohr, K. (2009). Single-cell-based image analysis of high-throughput cell array screens for quantification of viral infection. *Cytometry A* *75*, 309–318.
- McNab, F., Mayer-Barber, K., Sher, A., Wack, A., and O'Garra, A. (2015). Type I interferons in infectious disease. *Nat. Rev. Immunol.* *15*, 87–103.
- Navratil, V., de Chasse, B., Meyniel, L., Pradezynski, F., André, P., Rabourdin-Combe, C., and Lotteau, V. (2010). System-level comparison of protein-protein interactions between viruses and the human type I interferon system network. *J. Proteome Res.* *9*, 3527–3536.
- Nistal-Villán, E., Gack, M.U., Martínez-Delgado, G., Maharaj, N.P., Inn, K.S., Yang, H., Wang, R., Aggarwal, A.K., Jung, J.U., and García-Sastre, A. (2010). Negative role of RIG-I serine 8 phosphorylation in the regulation of interferon-beta production. *J. Biol. Chem.* *285*, 20252–20261.
- Patel, J.R., Jain, A., Chou, Y.Y., Baum, A., Ha, T., and García-Sastre, A. (2013). ATPase-driven oligomerization of RIG-I on RNA allows optimal activation of type-I interferon. *EMBO Rep.* *14*, 780–787.
- Pulloor, N.K., Nair, S., McCaffrey, K., Kostic, A.D., Bist, P., Weaver, J.D., Riley, A.M., Tyagi, R., Uchil, P.D., York, J.D., et al. (2014). Human genome-wide RNAi screen identifies an essential role for inositol pyrophosphates in Type-I interferon response. *PLoS Pathog.* *10*, e1003981.
- Razick, S., Magklaras, G., and Donaldson, I.M. (2008). iRefIndex: A consolidated protein interaction database with provenance. *BMC Bioinformatics* *9*, 405.
- Shang, T., Joseph, J., Hillard, C.J., and Kalyanaraman, B. (2005). Death-associated protein kinase as a sensor of mitochondrial membrane potential: Role of lysosome in mitochondrial toxin-induced cell death. *J. Biol. Chem.* *280*, 34644–34653.
- Shohat, G., Spivak-Kroizman, T., Cohen, O., Bialik, S., Shani, G., Berrisi, H., Eisenstein, M., and Kimchi, A. (2001). The pro-apoptotic function of death-associated protein kinase is controlled by a unique inhibitory autophosphorylation-based mechanism. *J. Biol. Chem.* *276*, 47460–47467.
- Shohat, G., Spivak-Kroizman, T., Eisenstein, M., and Kimchi, A. (2002). The regulation of death-associated protein (DAP) kinase in apoptosis. *Eur. Cytokine Netw.* *13*, 398–400.
- Smoot, M.E., Ono, K., Ruscheinski, J., Wang, P.L., and Ideker, T. (2011). Cytoscape 2.8: New features for data integration and network visualization. *Bioinformatics* *27*, 431–432.
- Steger, M., Tonelli, F., Ito, G., Davies, P., Trost, M., Vetter, M., Wachter, S., Lorentzen, E., Duddy, G., Wilson, S., et al. (2016). Phosphoproteomics reveals that Parkinson's disease kinase LRRK2 regulates a subset of Rab GTPases. *eLife* *5*, 5.
- Tejaro, J.R., Ng, C., Lee, A.M., Sullivan, B.M., Sheehan, K.C., Welch, M., Schreiber, R.D., de la Torre, J.C., and Oldstone, M.B. (2013). Persistent LCMV infection is controlled by blockade of type I interferon signaling. *Science* *340*, 207–211.
- Trinchieri, G. (2010). Type I interferon: Friend or foe? *J. Exp. Med.* *207*, 2053–2063.
- Tyanova, S., Temu, T., Sinitcyn, P., Carlson, A., Hein, M.Y., Geiger, T., Mann, M., and Cox, J. (2016). The Perseus computational platform for comprehensive analysis of (prote)omics data. *Nat. Methods* *13*, 731–740.
- Wies, E., Wang, M.K., Maharaj, N.P., Chen, K., Zhou, S., Finberg, R.W., and Gack, M.U. (2013). Dephosphorylation of the RNA sensors RIG-I and MDA5 by the phosphatase PP1 is essential for innate immune signaling. *Immunity* *38*, 437–449.
- Wilson, E.B., Yamada, D.H., Elsaesser, H., Herskovitz, J., Deng, J., Cheng, G., Aronow, B.J., Karp, C.L., and Brooks, D.G. (2013). Blockade of chronic type I interferon signaling to control persistent LCMV infection. *Science* *340*, 202–207.
- Wolf, A.J., Reyes, C.N., Liang, W., Becker, C., Shimada, K., Wheeler, M.L., Cho, H.C., Popescu, N.I., Coggeshall, K.M., Ardit, M., and Underhill, D.M. (2016). Hexokinase is an innate immune receptor for the detection of bacterial peptidoglycan. *Cell* *166*, 624–636.
- Ye, J., Coulouris, G., Zaretskaya, I., Cutcutache, I., Rozen, S., and Madden, T.L. (2012). Primer-BLAST: A tool to design target-specific primers for polymerase chain reaction. *BMC Bioinformatics* *13*, 134.
- Zhang, J., Hu, M.M., Shu, H.B., and Li, S. (2014). Death-associated protein kinase 1 is an IRF3/7-interacting protein that is involved in the cellular antiviral immune response. *Cell. Mol. Immunol.* *11*, 245–252.

STAR★METHODS

KEY RESOURCES TABLE

REAGENT or RESOURCE	SOURCE	IDENTIFIER
Antibodies		
mouse monoclonal anti- β -Actin	Sigma-Aldrich	A5441, RRID: AB_476744
mouse monoclonal anti-Influenza A NP (D67J), FITC-conjugate	Pierce/Thermo Scientific	MA1-7322, RRID: AB_1017747
rabbit polyclonal anti-Calnexin	Enzo Life Sciences	ADI-SPA-865-F, RRID: AB_11180747
rabbit polyclonal anti-DAPK1	Sigma-Aldrich	D1319, RRID: AB_1078622
mouse monoclonal anti-DAPK1	BD	610290, RRID: AB_397684
mouse monoclonal anti-GAPDH	Santa Cruz	sc-47724, RRID: AB_627678
goat polyclonal anti-human-IFN-beta	R&D Systems	AF814-SP
rabbit polyclonal anti-IFIT1	Abnova	H00003434-DO1
rabbit polyclonal anti-IRF3	Gift from Prof. Michael David (University of California, San Diego)	N/A
rabbit monoclonal anti-IRF7 (EPR4718)	Abcam	ab109255, RRID: AB_10866535
rabbit polyclonal anti-MAVS	Enzo Life Sciences	AT107
mouse monoclonal anti-phospho-pDAPK1 (pSer308)	Sigma-Aldrich	D4941, RRID: AB_476906
rabbit monoclonal anti-phospho-IRF-3 (pSer396)	Cell Signaling	4947, RRID: AB_823547
rabbit monoclonal anti-phospho-NAK/TBK1 (pS172)	Abcam	ab109272, RRID: AB_10862438
rabbit polyclonal anti-RIG-I	Enzo Life Sciences	ALX-210-932-C100, RRID: AB_2052506
Rabbit monoclonal anti-NAK/TBK1 (D1B4)	Cell Signaling	3504, RRID: AB_2255663
mouse monoclonal anti-TRADD (A-5)	Santa Cruz	sc-46653, RRID: AB_2209061
mouse monoclonal anti-HA (HA-7)	Sigma-Aldrich	H3663, RRID: AB_262051
rabbit polyclonal anti-c-Myc	Santa Cruz	sc-789, RRID: AB_631274
Chemicals, Peptides, and Recombinant Proteins		
OptiMEM	Thermo Scientific	31985070
Clarity Western ECL Substrate	Bio-Rad	170-5061
Calmodulin (Bovine)	Sigma-Aldrich	C4874
recombinant RIG-I	Jiang et al., 2011	N/A
High-Capacity cDNA Reverse Transcription Kit	Applied Biosystems	43-688-14
Coelenterazine	PJK, Germany	102173
D-Luciferin	PJK, Germany	102111
cOmplete Protease Inhibitor Cocktail Tablets	Roche	11873580001
Monoclonal anti-HA-agarose	Sigma-Aldrich	A2095
MagStrep "type2HC" beads, 5% suspension	IBA GmbH, Germany	2-1612-002
Effectene transfection reagent	QIAGEN	301427
HiPerFect transfection reagent	QIAGEN	301707
Lipofectamine 2000 transfection reagent	life technologies	11668019
RNAiMAX transfection reagent	life technologies	13778150
EasyTides ATP, [γ - 32 P]	Perkin Elmer	BLU502A250UC
Poly(C), polycytidilic acid, potassium salt	Sigma-Aldrich	P4903-10MG

(Continued on next page)

Continued

REAGENT or RESOURCE	SOURCE	IDENTIFIER
Poly(I:C), polyinosinic-polycytidylic acid, potassium salt	Sigma-Aldrich	P9582-50MG
Cytofix/Cytoperm	BD Biosciences	554722
iTaq Universal SYBR Green Supermix	Bio-Rad	17251525
Ribonucleotide Triphosphate Set	Roche	11277057001
RQ1 RNase-free DNase	Promega	M6101
Recombinant RNasin Ribonuclease Inhibitor	Promega	N2511
Critical Commercial Assays		
VeriKine-DIY™ Human Interferon Lambda ELISA	PBL	61840-1
LumiKine hIFN-β Xpress	Invivogen	luex-hifnb
Experimental Models: Cell Lines		
A549	University Hospital Heidelberg	N/A
A549 ^{AGO2}	Börner et al., 2013	N/A
A549 ^{RIG-I KO}	this publication	N/A
Huh7.5 ^{RIG-I}	Binder et al., 2011	N/A
Huh7.5 ^{RIG-I/eGFP-IRF3}	this publication	N/A
293T	Prof. Alexander Weber, University of Tübingen, Germany	N/A
293T ^{RIG-I}	this publication	N/A
Experimental Models: Organisms/Strains		
Influenza A Virus (A/WSN/33)	Prof. Georg Kochs, University Hospital Freiburg, Germany	N/A
Rift Valley fever virus ΔNSs Renilla (RVFVΔNSs_RLuc)	Prof. Friedemann Weber, University of Gießen, Germany	N/A
Sendai virus	Prof. Rainer Zawatzky, DKFZ, Heidelberg, Germany	N/A
Recombinant DNA		
pWPI based lentiviral vector	Binder et al., 2007	N/A
pcDNA6.2/nLumio-DEST	Thermo Scientific	12589016
pcDNA5/FRT/TO-N-strepHA	Dr. Andreas Pichlmair, Max-Planck-Institute for Biochemistry, Munich, Germany	N/A
pcDNA 3.1 (+)	Thermo Scientific	V79020
pGL3B/561 (IFIT1 promoter firefly luciferase reporter)	Prof. Ganes Sen, Cleveland Clinic, Cleveland, OH, USA	N/A
pRL-CMV	Promega	E2261
pRL-SV40	Promega	E2231
Lenti-CRISPR	Prof. Dr. Zeng, MIT, Cambridge, Massachusetts, USA (Addgene)	52961
other plasmids	This publication	see Table S1
Sequence-Based Reagents		
Silencer Human Kinase siRNA Library	Ambion	AM80010V3
primers	Sigma-Aldrich	see Tables S3 and S4
siRNAs	QIAGEN/MWG/Sigma-Aldrich	see Table S2
Software and Algorithms		
R	R Foundation for Statistical Computing	https://www.r-project.org/
Prism (v6)	GraphPad software	http://www.graphpad.com/scientific-software/prism/

(Continued on next page)

Continued

REAGENT or RESOURCE	SOURCE	IDENTIFIER
DAVID (v6.8)	Huang et al., 2009a, 2009b	https://david.ncicrf.gov/
Cytoscape (v3)	Smoot et al., 2011	http://www.cytoscape.org
LabImage 1D	INTAS/KAPELAN, Germany	http://www.kapelanbio.com/products/labimage/labimage-1d-2.html
MaxQuant version 1.5.3.2	Cox and Mann, 2008; Cox et al., 2011	http://www.biochem.mpg.de/5111795/maxquant
Perseus	Tyanova et al., 2016	http://www.biochem.mpg.de/5111810/perseus

CONTACT FOR REAGENT AND RESOURCE SHARING

For further details and requesting reagents described in this study, please contact the corresponding author Marco Binder (m.binder@dkfz.de, ORCID iD 0000-0002-5805-6109).

EXPERIMENTAL MODEL AND SUBJECT DETAILS**Cell lines**

A549 cells were obtained from the University Hospital Heidelberg. A549^{RIG-I KO} cells were generated by CRISPR/Cas9 technology using a lentiviral vector system and are based on a single cell clone. A549^{AGO2} cells stably overexpress a codon optimized variant of the human Argonaut 2 gene and were described previously (Börner et al., 2013).

293T cells were a gift from Prof. Alexander Weber, University of Tübingen, Germany. This line of 293T cells was tested to be virtually deficient for RIG-I, MDA5 and TLR3 and does not respond to double-stranded RNA transfected or added to the medium. For specific analysis of the RIG-I signaling pathway, RIG-I was reconstituted by lentiviral transduction, giving rise to 293T^{RIG-I} cells.

Huh7.5^{RIG-I} cells were generated and described previously in our lab (Binder et al., 2011). They are based on Huh7.5 cells, which were a kind gift from Charles M. Rice, Rockefeller University, New York City, USA.

All cell lines were tested for their authenticity by SNP-based multiplex human cell authentication (MCA) by Multiplexion GmbH, Immenstaad, Germany. Certificates are available upon request.

All cell lines were tested for contamination with mycoplasma (species specific for 14 different species, qualitative for > 100 species), Squirrel Monkey Retrovirus, Epstein-Barr-Virus and cross-contamination with material of human-, *Macaca cynomolgus*-, mouse-, rat-, Chinese hamster-, Syrian hamster-, feline-, canine-, rabbit-, pig, Guinea pig or *Drosophila* origin. Tests were performed by Multiplexion GmbH, Immenstaad, Germany. All cell lines were free of contaminations; certificates available upon request.

Primary cells

Primary mouse lung fibroblasts were prepared from female C57BL/6N mice (Charles River, Sulzfeld, Germany) kept under SPF conditions at the Heidelberg University mouse facility; see [Method Details](#) below.

Viruses

Influenza A virus (FLUAV), strain A/WSN/33 (H1N1), was a kind gift from Georg Kochs, University Hospital Freiburg, Germany. Virus stocks were grown on DF1 cells.

Renilla luciferase expressing Rift Valley fever virus (RVFV Δ NSs_RLuc), harboring a deletion of the NSs gene, which is replaced by the gene coding for *Renilla* luciferase, was generously provided by Friedemann Weber, University of Gießen, Germany. Virus stock were grown on BHK21 cells.

Sendai virus (SeV), prepared from allantoic fluid of embryonated chicken eggs, were a kind gift from Rainer Zawatzky, German Cancer Research Center (DKFZ, Heidelberg, Germany).

METHOD DETAILS**Cells and cell culture****General cell culture**

A549-, 293T- and Huh7.5-based cell lines were cultured in Dulbecco's modified Eagle medium (DMEM, Life Technologies, Germany) supplemented with 10% fetal calf serum (GE Healthcare, Germany / Sigma Aldrich, Germany), 100 μ g/ml penicillin, 100 μ g/ml streptomycin (Sigma Aldrich, Germany) and non-essential amino acids (Life Technologies, Germany). Cells were maintained in a humidified incubator with 5% CO₂ at 37°C.

Generation of primary cells

Primary mouse lung fibroblasts were generated from female C57BL/6N mice (Charles River, Sulzfeld, Germany). Lung tissue was cut into approx. 1 mm pieces and digested with Liberase TM (Sigma Aldrich, Germany) for 30 to 90 min at 37°C in DMEM. Liberase activity was stopped by washing 3 times with 10% FCS in DMEM. Digested lung pieces were cultured under above described culturing conditions for at least one week to allow fibroblasts to migrate out. Lung pieces and debris were then washed away and fibroblasts were trypsinized and passaged normally for a maximum of three passages.

Generation of stable cell lines

Stable cell lines were generated by lentiviral transduction. Briefly, lentiviral particles were produced on 293T cells by calcium phosphate transfection with the following three plasmids at a 3:1:3 ratio: (i) pCMV- Δ R8.91, coding for HIV gag-pol; (ii) pMD2.G, encoding the VSV-G glycoprotein; and (iii) a lentiviral vector based on the pWPI vector harboring the gene of interest or lenti-CRISPR-RIG-I. pCMV- Δ R8.91 and pMD2.G and pWPI were kind gifts from Prof. Didier Trono (Lausanne, Switzerland). Cell-free supernatants were harvested 48, 56 and 72 hr after transfection and used for transduction of target cells. Successfully transduced cells were selected by supplementing the culture medium with 5 μ g/ml blasticidin, 1 μ g/ml puromycin or 1 μ g/ml geneticin (G418).

siRNA screening

Primary screen

Cell arrays were prepared by printing Ambion Silencer Human Kinase siRNA Library (AM80010V3) and Lipofectamine 2000 (Life Technologies) on LabTek chamber slides (Thermo Scientific, Germany) as described before (Erflie et al., 2007). The library covered 719 genes with three siRNAs per gene. Huh7.5^{RIG-I} cells were stably transduced with an N-terminal fusion of IRF3 with eGFP to yield Huh7.5^{RIG-I/eGFP-IRF3}. Cells were seeded on cell arrays at a density of 2×10^5 cells per chamber slide and were stimulated 48 hr post seeding by transfection of 500 ng poly(I:C), 3 μ g poly(C) and 13 μ l of Lipofectamine 2000 according to the manufacturer's protocol. Cells were fixed with 4% paraformaldehyde 2 hr after poly(I:C) transfection and nuclei were stained using Hoechst 33342. Cell arrays were imaged using the automated IX81 inverted screening microscope (Olympus). Screening was performed in 12 replicates. Acquired images underwent automated and manual quality control to exclude areas of aberrant staining. Then, the images were automatically analyzed using an adaption of the image analysis method by Matula and colleagues (Matula et al., 2009), which comprises segmentation of cell nuclei and quantification of mean GFP signal intensities within the nuclei and in a 6 pixel region surrounding the nucleus (i.e., cytoplasmic signal).

Bioinformatics analyses

Functional annotation clustering was performed using the online analysis tool DAVID (Huang da et al., 2009a, b) version 6.8, with the 104 primary hit candidates as a query dataset and the 719 genes from the library defining the background.

Protein-protein-interaction (PPI) network analyses of hit candidates were performed on a human interactome map. The full interactome was generated based on a download of iRefIndex 9.0 (Razick et al., 2008), post-processed in several steps including filter applications in order to reconstruct a high-quality human interactome. As an example, only protein-protein interactions found at least twice (in two distinct publications or through two distinct experimental methods) were retained. This allowed to dramatically improve the trustworthiness of the full network. The IFN-related network is an update of the earlier published network (de Chassesey et al., 2012). Protein interaction networks were visualized with Cytoscape (Smoot et al., 2011). Enrichment analysis of hits in lists of host factor genes for different viruses was based on lists assembled in previous work (de Chassesey et al., 2012). In all cases, Exact Fisher tests assessing the significance of hit-related proportions were performed using the kinome siRNA library as background.

Validation screens

From the primary hit candidates, 58 top ranking genes (based on p values < 0.05 or prior knowledge from literature) were chosen for secondary validation screening. Three different rounds of validation screening have been performed using cell lines, readouts and siRNAs distinct from the primary screen. Two siRNAs per gene were ordered from QIAGEN (Hilden, Germany); QIAGEN siRNA IDs can be found in [Data S1](#). Transfection of siRNA was done using HiPerfect (QIAGEN) according to the manufacturer's protocol.

Validation screen 1 – VSV vRNA: In 9 biological replicates, 293T^{RIG-I} cells (at 7000 cells/well, 96-well format) were transfected with 10 nM siRNA. 48 hr later cells were transfected with IFIT1 promoter firefly luciferase and SV40-early promoter *Renilla* luciferase reporter plasmids by Effectene (QIAGEN). 8 hr later cells were stimulated with 40 ng/well Vesicular Stomatitis virus (VSV) vRNA (RNA prepared from VSV containing culture supernatants). 16 hr post stimulation, cells were lysed and luciferase activity was measured.

Validation screen 2 – RIG-I^{2CARD}: In 9 biological replicates, constitutively signaling 293T^{RIG-I2CARD} cells (7000 cells/well, 96-well format) were transfected with 10nM siRNA. 48 hr later cells were transfected with IFIT1 promoter firefly luciferase and SV40-early promoter *Renilla* luciferase reporter plasmids by Effectene (QIAGEN). 24 hr post reporter transfection cells were lysed and luciferase activity was measured.

Validation screen 3 – RVFV: In 9 biological replicates, A549^{AGO2} cells (Börner et al., 2013) (7000 cells/well, 96-well format) were transfected with 10nM siRNA. 48 hr later cells were infected with RVFV Δ NSs_RLuc (MOI 0.01) for additional 48 hr before they were lysed and *Renilla* luciferase activity was measured.

Cloning and plasmids

Expression constructs of hit genes

Expression constructs for hit genes were either taken from the ORFeome library, were kind gifts of generous colleagues or were cloned from cells by RT-PCR. Final constructs contained an affinity tag (V5, HA, Myc or Flag) and were under transcriptional control of the CMV promoter. For details, see [Table S1](#).

DAPK1 truncations and point mutants

Truncations, domain deletions and point mutants of DAPK1 are based on the above mentioned CMV-driven expression construct (pcDNA) and were cloned using overlap PCR with the primers listed in [Table S4](#). For internal deletions or point mutations indicated overlap primers were used in combination with forward and reverse primers for full-length DAPK1 or KD + CaM + Ank Reverse primer in case of KD + CaM + Ank S308A/D and K42A.

RIG-I point mutants

RIG-I phosphomutants were generated by whole plasmid mutagenesis using the primers listed in [Table S4](#) and pENTR221-RIG-I. Only S8 mutants were cloned via BP clonase II into pDONR207.

pWPI based lentiviral vectors

For stable expression, described vectors have been used for RIG-I and eGFP-IRF3 (ref). For reconstitution of A549^{RIG-I KO} cells RIG-I WT and RIG-I mutants were cloned by LR reaction using LR clonase II (life technology) into a gateway compatible pWPI. Expression from pWPI vectors is driven by an EF1- α promoter.

Lenti-CRISPR-RIG-I vector

RIG-I specific gRNA (CTGTTGGAGCTCCAGGAGGA) was cloned into the lenti-CRISPR plasmid (Addgene #52961) via BsmBI to generate lenti-CRISPR-RIG-I.

Gene silencing by siRNA

Cells were seeded in 24-well plates and subsequently transfected by RNAiMax (Invitrogen) with a final concentration of 10 nM siRNA. siRNAs for validation screening were purchased from QIAGEN; QIAGEN siRNA IDs are listed in [Data S1](#). For all further characterization experiments beyond screening, those siRNAs yielding the strongest effect in validation screening, respectively, were chosen (listed in [Table S2](#)). Additional mouse and human DAPK1 siRNA were purchased from Sigma-Aldrich (listed in [Table S2](#)) 48 hr post transfection cells were transfected with IFIT1 promoter (IRF3) or NF κ B luciferase reporter or left untreated for mRNA measurements. 8 hr later cells were stimulated for further 16 hr, before cells were lysed and subjected to mRNA quantification or measuring of luciferase activity (see “RIG-I signaling assays” below).

Overexpression of hit genes

293T^{RIG-I} or 293T cells (1.5×10^5 cells/well, 24-well format) were transfected with Lipofectamine 2000 (Invitrogen) 24 hr after seeding with the indicated amounts of CMV-promoter driven expression plasmids (supplemented with empty pcDNA plasmid to yield a final concentration of 1 μ g of DNA per 2 μ l of Lipofectamine 2000 per well) without or with IFIT1 promoter (IRF3) or NF κ B firefly luciferase and SV40-early promoter *Renilla* luciferase reporter plasmids. 8 hr post transfection cells were stimulated for further 16 hr, before cells were lysed and luciferase activity measured (see “RIG-I signaling assays” below).

RIG-I signaling assays

Stimulation of cells

Untreated, siRNA-transfected (see above) or expression-plasmid-transfected (see above) cells were transfected with 400 ng poly(I:C) or 10 ng 200 bp 5'ppp-dsRNA ([Binder et al., 2011](#)) using Lipofectamine 2000 (Invitrogen). For the Lipofectamine 2000 transfection mix, stimulatory RNA (poly(I:C) or 5'ppp-dsRNA) was mixed with non-stimulatory poly(C) to yield a constant end-concentration of 500 ng of RNA per 1 μ l Lipofectamine 2000 per well.

Readout by luciferase reporter assay

IRF3 or NF κ B activation was measured using the promoter luciferase reporter constructs pGL3B/561 (kind gift of Ganes Sen, Cleveland) or pGL4.32[luc2P/NF κ B-RE/Hygro] (Promega), respectively. Reporter plasmids were co-transfected with pRL-SV40 for normalization and the stimulatory RNA during stimulation of cells (see above), if not stated otherwise. For the luciferase assay (24-well format), stimulated cells were lysed in 100 μ l luciferase lysis buffer (1% Triton X-100, 25 mM glycyl-glycin [pH 7.8], 15 mM MgSO₄, 4 mM EGTA, 10% glycerol [99%]) directly in the well. Plates were frozen and stored at -80°C until measurement. Firefly luciferase was measured applying 400 μ l luciferase assay buffer (15 mM K₃PO₄ [pH 7.8], 25 mM glycyl-glycin [pH 7.8], 15 mM MgSO₄, 4 mM EGTA) with freshly added 1 mM DTT, 2 mM ATP and 1 mM *D*-Luciferin. *Renilla* luciferase was measured after firefly, applying 400 μ l luciferase assay buffer supplemented with 1.43 μ M coelenterazine (PJK, Germany) and using a 480 nm filter (480m20BREThs, Berthold) to exclude the firefly signal. After measurement of *Renilla*, luciferase activity was quenched by addition of 100 μ l of 10% SDS to prevent bleedthrough into the neighboring wells. Measurements were performed using a Mitras² multimode plate reader LB942 (Berthold, Germany). Firefly luciferase, reporting IRF3 and NF κ B activation, was normalized to respective *Renilla* value to normalize for transfection efficiency and cell numbers.

Readout by quantitative RT-PCR

To assess IRF3 activation in the absence of artificial promoter reporters, transcription of endogenous IFIT1 or IFN- β genes was measured by quantitative RT-PCR. Total RNA was isolated from stimulated cells using the NucleoSpin RNA Kit (Macherey-Nagel) according to manufacturer's protocol. For cDNA generation, 1 μ g of total RNA was used and reverse transcribed with the High-Capacity cDNA Reverse Transcription Kit (Applied Biosystems) according to manufacturer's instructions by using a thermal cycler. Quantitative real-time PCR was performed with SYBR Green (Biorad) and gene-specific primers (see [Table S3](#)) using the CFX96 real-time system (Biorad). Primers were designed using PrimerBlast ([Ye et al., 2012](#)) and requiring exon-exon junction overlap. mRNA levels were normalized to GAPDH and relative levels were determined using the $\Delta\Delta C_t$ method.

Readout by immunoblot

In order to determine IFN- β and IFIT1 protein expression infected or stimulated cells were lysed in Laemmli sample buffer. Proteins were detected as described in "Immunoblotting" and quantifications were performed as described in "Quantitative immunoblot analysis."

Readout by ELISA

IFN λ 1–3 was measured in the supernatant of FLUAV infected cells 32 hr post infection using a IFN λ 1–3 ELISA kit (PBL-Interferon source, USA) according to the manufacturer's instructions.

Secreted IFN- β from siDAPK1_2 silenced and 5' ppp-dsRNA transfected A549 cells were measured using a IFN- β ELISA kit (LumiKine Xpress hIFN- β , InvivoGen, USA) according to the manufacturer's instruction. For accumulative measurements, supernatants were kept on the cells from the start of stimulation until the indicated time point. For measuring secretion rates, medium was changed 1 hr prior to the indicated time point.

RIG-I pathway probing with influenza virus

Influenza A virus infection

For gene silencing studies, A549 cells were transfected with the indicated siRNAs and incubated for 40 hr before virus infection. A549 or A549-derived cells were infected with influenza A virus (A/WSN/33) at an MOI of 0.01 (MOI of 0.001 for titration assay) in OptiMEM for 1 hr. Inoculum was taken off and replaced by fresh cell culture medium. 32 hr post infection (flow cytometry and microscopy) or 48 hr post infection (titer determination) cells or supernatants, respectively, were harvested and analyzed (see below).

Readout by TCID₅₀ determination

A549 cells were seeded at 7000 cell/well, in 96-well format. The top row of wells was infected with a 1:100 pre-dilution of virus containing supernatants (see above), and the further rows were infected with serial dilutions (1:5). Cells were then incubated for 72 hr to allow for virus-dependent cell death to occur. Per-well cytotoxicity was determined and TCID₅₀ was calculated using the Spearman and Kaerber based TCID₅₀ calculator (<https://www.klinikum.uni-heidelberg.de/Downloads.126386.0.html>).

Readout by flow cytometry

Influenza infected A549 or A549-derived cells were washed with PBS and trypsinized (0.05% trypsin, 0.02% EDTA), trypsin was stopped by adding FCS containing DMEM. Cells were washed again with PBS. Cell pellets were carefully suspended in 100 μ L Cytofix/Cytoperm (BD Biosciences) and incubated for 20 min on ice. Cells were washed twice with 1 mL Perm/Wash solution and then stained in 50 μ L of 1:50 diluted FITC-coupled anti-Influenza A NP antibody (Pierce) in Perm/Wash for 30 min on ice. Cells were washed twice with 1 mL Perm/Wash solution and transferred into PBS. In IFIT1 co-stained samples IFIT1 antibody (Abnova) 1:500 was added together with anti-Influenza NP antibody. After two wash steps, cells were incubated with 1:1000 anti-rabbit Alexa Fluor 647 (Fisher Scientific) secondary antibody for 30 min on ice. Subsequently, samples were washed three times with 1 mL Perm/Wash solution and transferred into PBS. Stained samples were measured on the same day using FACSCalibur and CellQuest (BD Biosciences) or LSRFortessa (BD Bioscience) and FlowJo (FlowJo, LLC).

Readout by immunofluorescence microscopy

Influenza virus infected A549 cells on glass coverslips were fixed using 4% paraformaldehyde for 20 min and were stained with 1:50 diluted FITC-coupled anti-Influenza A NP antibody (Pierce) for 45 min. Subsequently nuclei were stained with DAPI (MoBiTec). Pictures were taken on a Keyence BZ 9000 Imager (Keyence).

Immunoblotting

Cells were lysed using NP40 lysis buffer (20 mM TRIS [pH 7.6], 100 mM NaCl, 1% NP40, 50 mM NaF, Protease inhibitor [Roche, Germany]). Post-nuclear fractions were mixed with 6x sample buffer (0.1M TRIS [pH 6.8], 30% glycerol, 3% SDS, 7.5% β -mercaptoethanol, 0.06% bromophenol blue) or lysed directly in 1 x sample buffer and were separated on 8% or 12% (for IFN- β) SDS-PAGE. Proteins were subsequently transferred to PVDF membrane or nitrocellulose (for IFN- β) and detected by using anti-HA, anti-Myc, anti-V5, RIG-I, MAVS, TBK1, IKK ϵ , IRF3, DAPK1, phosphor-DAPK1(pS308), IFIT1 or IFN- β (antibodies are listed in [Key Resources Table](#)). Primary antibodies were detected using secondary HRP conjugated goat anti-mouse or anti-rabbit antibodies (Sigma Aldrich). Immunoblots were incubated with Clarity ECL substrate (Biorad) or ECL Prime (GE Life Sciences) and signals were detected with a high-sensitivity CCD camera (ChemoCam Imager 3.2, INTAS, Germany).

Immunoprecipitation

Stimulated cells (see above) were lysed in 750 μ l / 1000 μ l of lysis buffer (20mM TRIS [pH7.6], 100 mM NaCl, 1% NP40, 50 mM NaF, protease inhibitor cocktail [Roche]) for 30 min on ice and nuclei were spun down at 4°C, 18000 g for 30 min. The post-nuclear fraction was incubated with 20 μ l pre-washed monoclonal anti-HA agarose beads (Sigma Aldrich) for 4 hr at 4°C. Beads were washed with lysis buffer 3 times for 15 min at 4°C. Beads were additionally washed twice with pre-chilled PBS. Proteins were eluted by addition of 200 μ l of 5% SDS in PBS for 10 min shaking (1100 rpm) at room temperature. Eluted proteins were precipitated by adding 800 μ l ice cold acetone. The pellet was resolved in sample buffer and subjected to immunoblot analysis (see above).

RNA immunoprecipitation

6x10⁵ 293T cells were transfected using Lipofectamine 2000 (Invitrogen) with YFP, Strep-HA-RIG-I^{WT}, Strep-HA-RIG-I^{T667E}, Strep-HA-RIG-I^{T667E/T671E} or Strep-HA-RIG-I^{cluster-I \rightarrow E}. 24 hr after transfection cells were lysed in RIP lysis buffer (150 mM KCl, 25 mM TRIS [pH7.5], 5 mM EDTA, 0.5 mM DTT, 0.5% NP40, protease inhibitor cocktail [Roche] and RNasin [Promega]). 50 ng of 200 bp 5'ppp-dsRNA (Binder et al., 2011) was added to the samples and incubated for 30min at 4°C while rotating. Subsequently, a Strep-tag pulldown was performed according to the manufacturer's instruction (IBA, Göttingen, Germany). RNA was isolated from the eluates using the NucleoSpin RNA kit (Macherey-Nagel, Germany) and co-purified dsRNA amounts were measured via quantitative RT-PCR (see above, primers listed in Table S3).

RIG-I phosphorylation assays

In vitro phosphorylation assay

1x10⁷ 293T cells were seeded on a 15 cm-dish. On the next day cells were transfected with 62 μ g of plasmid encoding N-terminal Strep-HA-DAPK1^{Kin|CaM|Ank}, Strep-HA-DAPK1^{Kin|CaM|Ank (K42A)} or YFP via calcium phosphate transfection. 8 hr later medium was replaced by fresh cell culture medium. 48 hr post transfection cells were lysed in high salt NP40 lysis buffer (20 mM TRIS [pH 7.6], 300 mM NaCl, 1% NP40, 50 mM NaF, Protease inhibitor [Roche]). Post nuclear fractions were subjected to MagStrep "type2" beads (IBA, Göttingen, Germany) and pulldown was performed according to the manufacturer's protocol. Purified samples were mixed with 1 μ g of recombinant RIG-I (Jiang et al., 2011) in kinase assay buffer (50 mM HEPES, 20 mM MgCl₂, 0.5 mM CaCl₂ [pH 7.5]) and assays were further supplemented with 1 mg/ml BSA and 1 μ M bovine calmodulin (Sigma Aldrich). Reaction was started by adding 50 μ M ATP spiked with 10 μ Ci of γ -³²P-ATP (2 pmol). Assay was incubated for 20 min at 30°C and was subsequently stopped by adding 6x sample buffer (0.1 M TRIS [pH 6.8], 30% glycerol, 3% SDS, 7.5% β -mercaptoethanol, 0.06% bromophenol blue). Samples were separated on an 8% SDS-PAGE and transferred onto PVDF membrane. ³²P was detected using a phosphor screen and a Storm 860 molecular imager (GE Healthcare). Total DAPK1 and RIG-I levels were detected using western blot analysis.

Phospho-site determination by mass spectrometry

Sample preparation and LC/MS-MS analysis was performed as described previously (Habjan et al., 2013). Briefly, *in vitro* phosphorylation assay reactions (see above, non-radioactive ATP) were stopped by adding SDS lysis buffer (4% SDS, 10 mM Tris [pH 7.5]), boiled, sonicated, reduced with 10mM DTT, alkylated with 55mM iodoacetamide and precipitated with ice-cold acetone (v/v = 80%) overnight. Pellets were dissolved in U/T buffer (6 M urea, 2 M thiorurea, 50 mM Tris [pH 8.0]), digested with LysC and trypsin (1:100) and C18 desalted peptides analyzed by LC-MS/MS on a Q Exactive Plus instrument (Thermo Fisher Scientific). Peptides were loaded on a 50 cm reversed phase column (packed in-house with ReproSil-Pur C18-AQ 1.9 μ m resin [Dr. Maisch GmbH]) and separated with buffer A (0.1% formic acid) and buffer B (80% acetonitrile, 0.1% formic acid) on an EASY-nLC 1000 system (Thermo Fisher Scientific) and eluted with a gradient of 5%–30% buffer B over 95 min followed by 30%–95% buffer B over 10 min as described previously (Steger et al., 2016). The mass spectrometer was programmed to fragment Top15 ions.

QUANTIFICATION AND STATISTICAL ANALYSIS

Analysis of primary siRNA screen

Cell activation ratios were computed as ratio of nuclear to cytoplasmic signal per cell. Activation ratios were subsequently normalized for local cell population context and were further used to compute active cell enrichment scores and p values per siRNA spot, as we have previously described (Knapp et al., 2011). Combined p values were computed on enrichment scores averaged across replicates. siRNAs with a combined p value < 0.05 were considered hit candidates.

Analysis of secondary siRNA screens

Validation screens were analyzed using R 3.3.0 (<http://www.R-project.org>). Nine replicates were loaded and data for each siRNA were combined, and the 10% most extreme values per siRNA (i.e., outliers) were removed. Significance was tested against the non-targeting siRNA as a negative control using two-tailed, unpaired Student's t test. Results were plotted using the boxplot function, with colors coding for the respective p value. Descriptive statistics (p values, Z-scores) are given in Data S1.

Quantitative immunoblot analysis

For quantitative immunoblot analyses, blots were incubated with ECL substrate (see above) and recorded using a high-sensitivity, high-dynamic range CCD camera system (ChemoCam Imager 3.2, INTAS, Germany) without binning at 16-bit / pixel. Luminescence

signals were quantified using the LabImage 1D software (INTAS, Germany), using intensity profiles with local background correction. All specific signals were normalized to the respective loading control.

Analysis of mass-spectrometry data

Raw MS data were processed using MaxQuant version 1.5.3.2 (Cox and Mann, 2008; Cox et al., 2011). Searches were performed against human UniProt FASTA database (UniprotKB, release 2014_09). The search included phosphorylation of Ser, Thr, Tyr residue (PhosphoSTY) as variable modifications. Quantification was performed by MaxQuant, with label-free quantification (LFQ) algorithm (Cox et al., 2011) and 'match between runs' enabled. Bioinformatic analyses were performed in Perseus (<http://www.perseus-framework.org>) and Microsoft Excel and data visualized using GraphPad Prism7 (GraphPad Software) and Illustrator (Adobe). Heatmap of phosphosites was built on logarithmized (\log_2) intensities.

General statistical testing

Statistical testing was performed as indicated in the text and figure legends. If not stated otherwise, testing was performed using two-tailed, non-paired Student's t test in the GraphPad Prism v6 software. Significance levels used were: non-significant (n.s., $p > 0.05$), * ($p \leq 0.05$), ** ($p \leq 0.01$), *** ($p \leq 0.001$) and **** ($p \leq 0.0001$).

DATA AND SOFTWARE AVAILABILITY

Data from siRNA screening are provided in [Data S1](#).

Molecular Cell, Volume 65

Supplemental Information

Phosphorylation-Dependent Feedback

Inhibition of RIG-I by DAPK1 Identified

by Kinome-wide siRNA Screening

Joschka Willemsen, Oliver Wicht, Julia C. Wolanski, Nina Baur, Sandra Bastian, Darya A. Haas, Petr Matula, Bettina Knapp, Laurène Meyniel-Schicklin, Chen Wang, Ralf Bartenschlager, Volker Lohmann, Karl Rohr, Holger Erfle, Lars Kaderali, Joseph Marcotrigiano, Andreas Pichlmair, and Marco Binder

identified. Homotypic interaction (homodimerization) were ignored. **(B)** Network analysis of the high-confidence hit DAPK1. All direct interaction partners represented in the interactome are displayed and labeled. Further hit candidates that interact with at least one of these DAPK1-interactors are displayed in turquoise and labeled. **(C)** Graphical representation of the interferon-related protein-protein-interaction network. Four hit candidates are found to be members of this network (colored turquoise). Using a curated full human interactome, further primary hit candidates that interact with members of the interferon network were identified and arranged in a circle around the interferon network (turquoise), with their direct interaction partners colored orange.

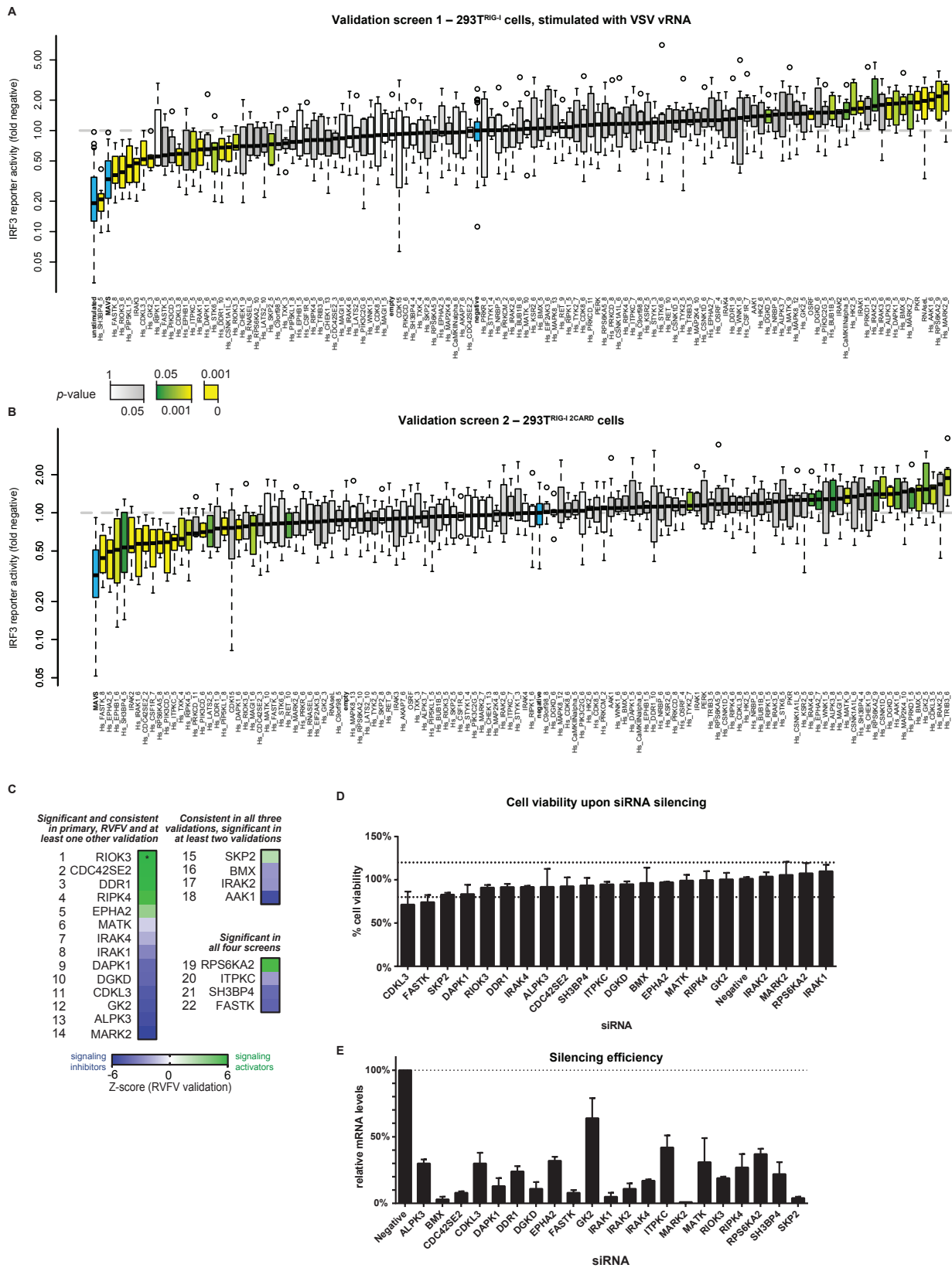


Figure S2. Validation of 22 Hits in Secondary Screen, Related to Figure 1 and 2. Fifty-eight candidate genes from primary screen were subjected to three rounds of secondary validation screening with two siRNA per gene (Qiagen siRNA ID indicated in figure); details in STAR

Methods . **(A)** Validation screen 1 was performed in 293T^{RIG-I} cells, stimulated by transfection of VSV vRNA and read out by IRF3 activity luciferase reporter. **(B)** Validation screen 2 was performed in constitutively signaling 293T^{RIG-I 2CARD} cells. Read out was IRF3 activity luciferase reporter. Validation screen 3 was performed in A549^{Ago2} cells that were infected with *Renilla* luciferase expressing Rift Valley fever virus (RVFV Δ NSs), which triggers the RIG-I response very efficiently and at the same time is highly sensitive to interferon. Results are displayed in figure 1D of the main text. **(A,B)** From nine biological replicates, the most extreme of each siRNA was removed and results were normalized to non-targeting siRNA. Significance was tested against non-targeting siRNA by Student's t-test and *p*-values were color-coded, scale included in figure. **(C)** Twenty-two candidate genes were validated in secondary screening by fulfilling the hit calling criteria indicated in the figure (see also STAR methods). The magnitude of the effect (Z-score) of their knockdown in validation round 3 (RVFV) is color-coded, scale included in panel. Hits can be classified according to the direction of their effect: genes whose knockdown *increased* IRF3 activation upon RIG-I stimulation are considered *signaling inhibitors* (i.e. their presence inhibits RIG-I/IRF3 signaling); genes whose knockdown *decreases* IRF3 activation are considered *signaling activators*. For each gene, the siRNA yielding the biggest effect in validation screening was chosen for further characterization of the respective gene (see figure 2). Cytotoxic effects **(D)** and silencing efficiency **(E)** were measured by ATP quantification and gene-specific qRT-PCR, respectively.

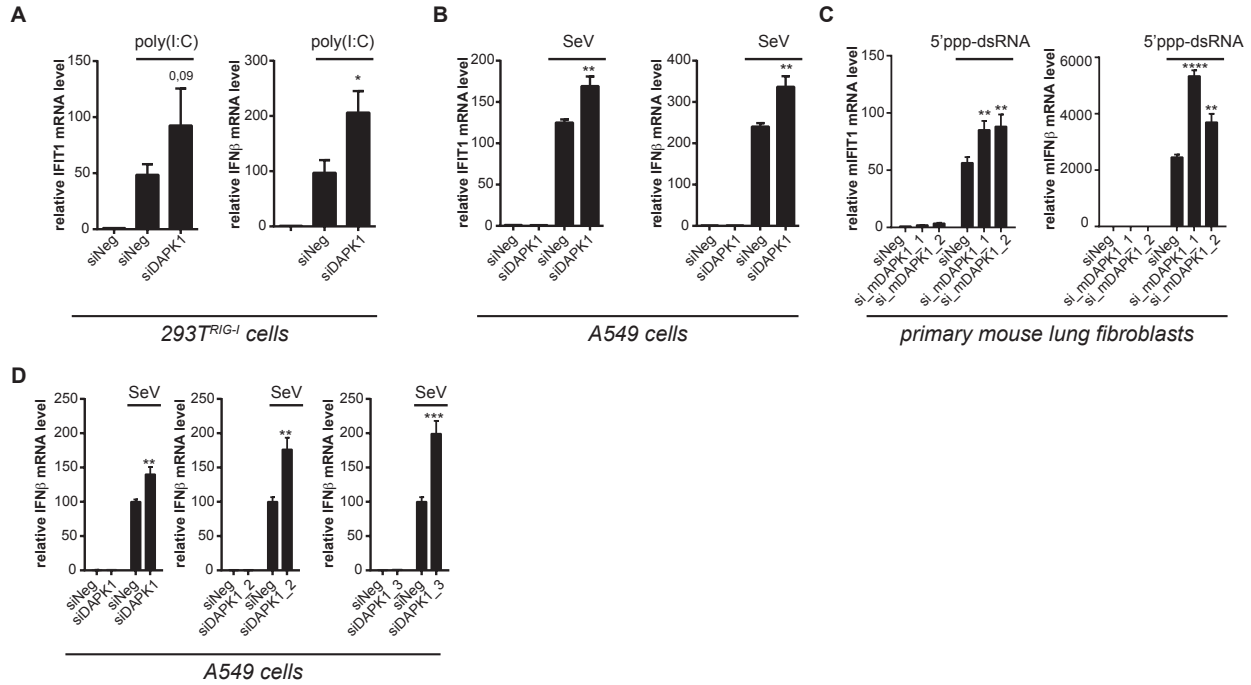


Figure S3. Knockdown of DAPK1 in Different Cell Types and With Different siRNAs, Related to Figure 3. DAPK1 was silenced by siRNA in three different human cell lines: Huh7.5 (primary screen), 293T^{RIG-I} cells (**A**, and main figure 3D) and A549 cells (**B**). To assess species-specificity of the effect, primary mouse fibroblasts from lung tissue were generated and transfected with mouse-specific DAPK1 siRNAs as indicated (**C**). Cells were either non-stimulated (left bars) or stimulated with the indicated stimulus (right bars), read-out was IFIT1- or IFNβ-mRNA levels, measured by gene- and species-specific qRT-PCR. (**D**) Comparison of three further siRNAs (from a different vendor) targeting human DAPK1 was performed in A549 cells stimulated with Sendai virus (SeV). Figure shows one representative of two (panel C) or three (panels A, B and D) independent experiments. Values represent mean +/- SD of triplicate values.

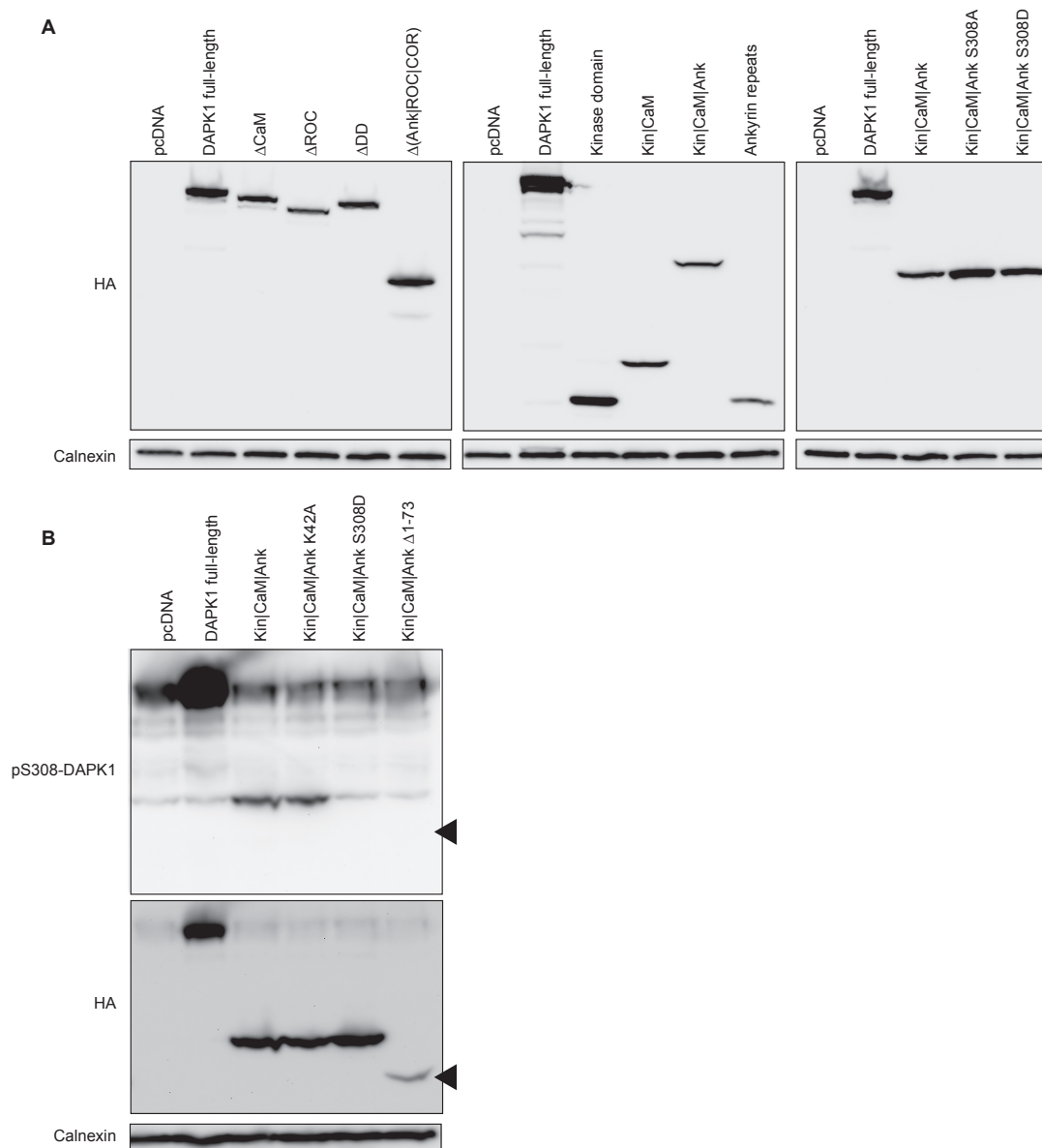


Figure S4. DAPK1 Domain Mapping Expression Controls, Related to Figure 4. (A, B)

Truncated DAPK1 variants were expressed in 293T^{RIG-I} cells and checked for their effect on RIG-I induced IRF3 activation. **(A)** To rule out artifacts owing to a lack of expression, protein was detected using anti-HA immunoblotting. Calnexin was stained as a loading control. **(B)** In order to monitor kinase activity of the tested DAPK1 mutants cells were treated with 100nM of the phosphatase inhibitor Calyculin A for 30min and phosphorylation at S308 was detected by immunoblotting along with total protein amounts by HA staining und calnexin as a loading control. Figure shows one representative out of at least three independent experiments.

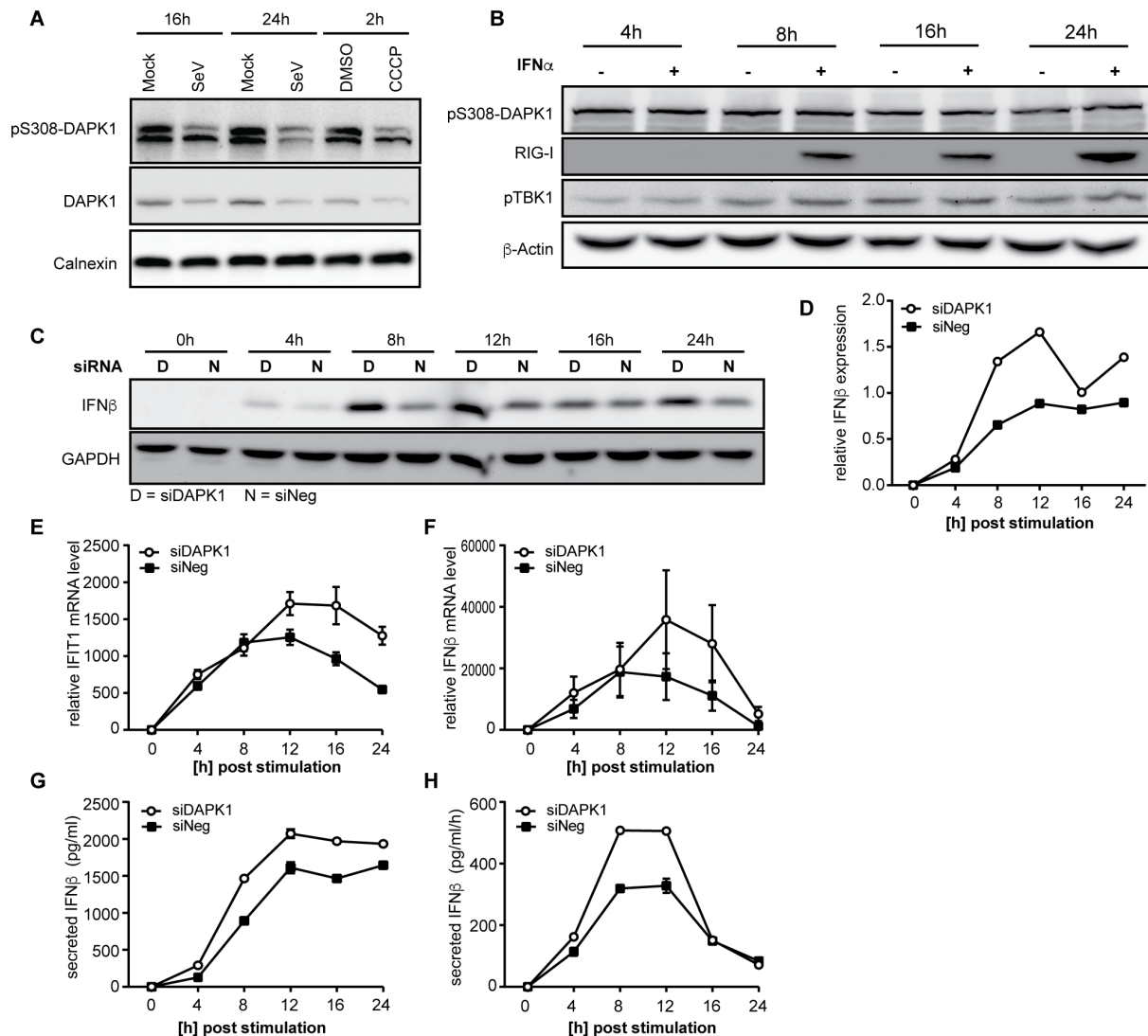


Figure S5. DAPK1 Activation upon Virus Infection and IFN β Production upon DAPK1 Silencing, Related to Figure 5. (A) A549 cells were infected with Sendai virus (SeV) for the indicated amounts of time (or treated with the protonophore CCCP as a positive control) and then lysed and analyzed for DAPK1 phosphorylation at site S308 and DAPK1 total levels. Calnexin was stained as a loading control. SeV infection activated DAPK1 similarly to the positive control and similarly to RIG-I stimulation by 5'ppp-dsRNA (main figure 5). **(B)** A549 cells stimulated with 100 IU/ml IFN α for the indicated amount of time and then lysed and analyzed for phosphorylation of DAPK1 at S308. RIG-I was stained as an indicator for IFN stimulation and calnexin as a loading control. **(C–H)** Analysis of mock- or DAPK1-silenced (siDAPK1_1) A549 cells stimulated by transfection of 5'ppp-dsRNA for the indicated time span (0–24 h). IFN β induction was detected by immunoblotting from cell lysates **(C)** (densitometric quantification of IFN β signal normalized to GAPDH is shown in panel **D**) or by ELISA from culture supernatants after the indicated time **(G, accumulated levels in pg/ml)** or from supernatants that had been changed to fresh medium 1 h prior to the indicated time point **(H, secretion rate in pg/ml/h)**. IFN β and IFIT1 mRNA levels were analyzed by qRT-PCR **(E and F)**. Figure shows one representative out of three **(A, C–H)** or two **(B)** independent experiments.

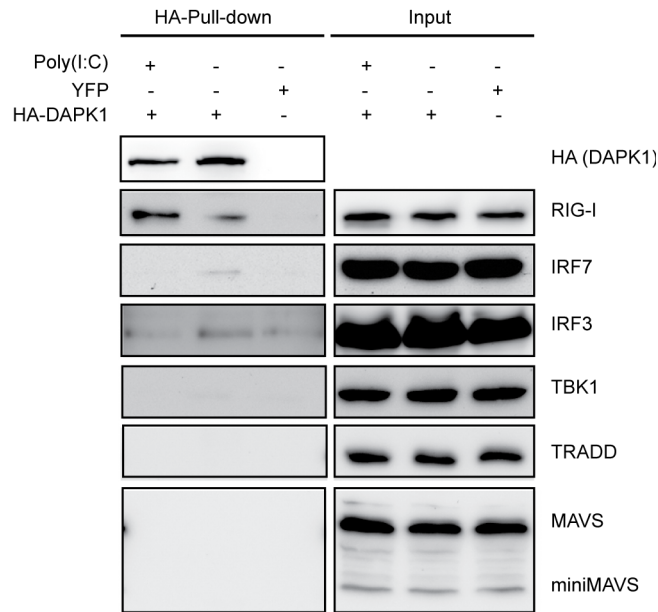


Figure S6. Co-Precipitation of RIG-I Pathway Members with DAPK1, Related to Figure 6.

293T^{RIG-I} cells were transfected with HA-tagged DAPK1 or YFP for 48 h. Cell lysates were used for HA-immunoprecipitation and analyzed by immunoblotting with antibodies against the indicated proteins. The co-precipitation with IRF7 could not be reliably reproduced in repetitions of the experiment; RIG-I co-precipitation was the strongest and only reliable interaction detected. Figure shows one representative out of three independent experiments.

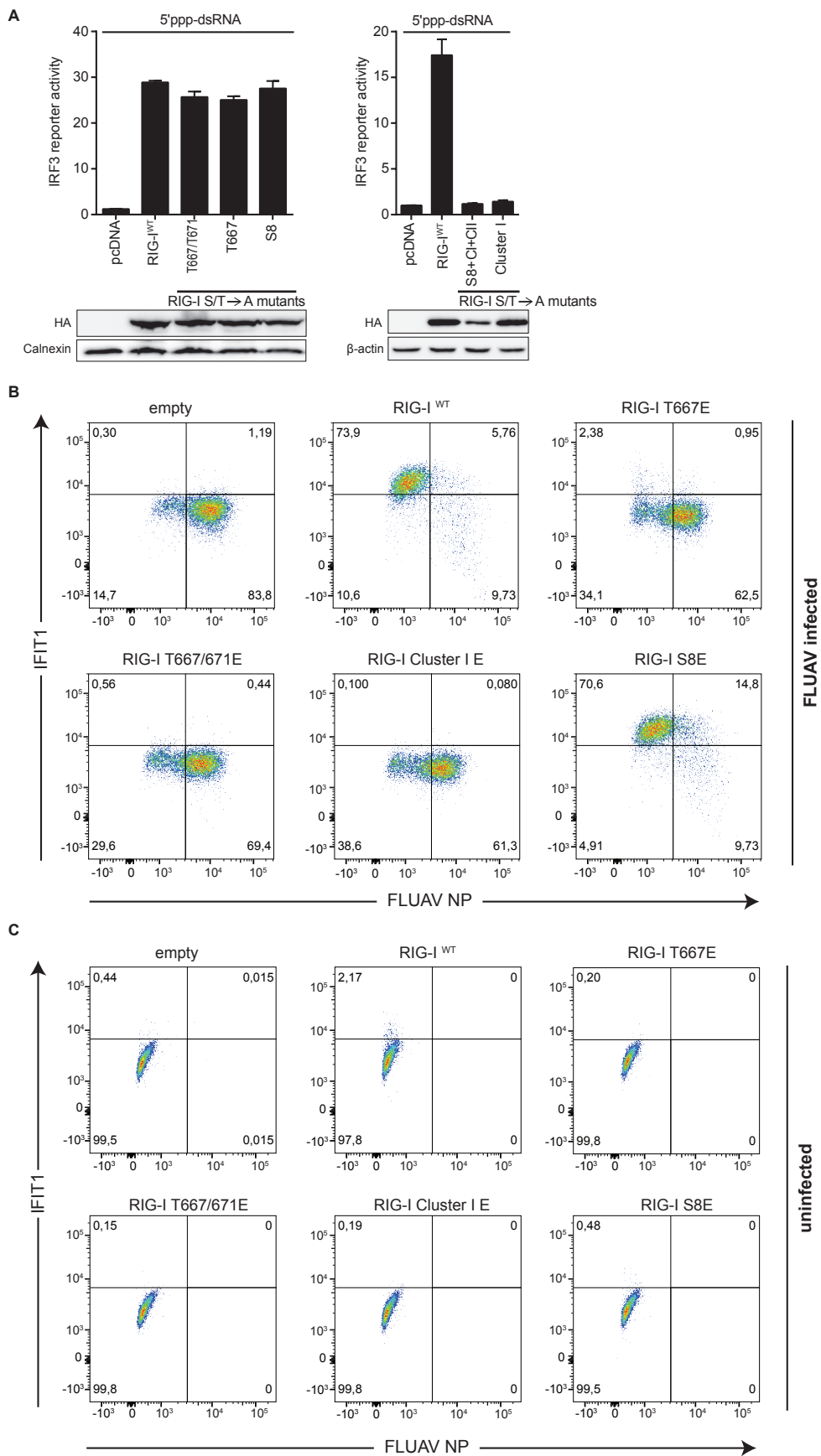


Figure S7. Phosphorylation Mutants of RIG-I, Related to Figure 7. RIG-I residues phosphorylated by DAPK1 were replaced with phosphomimetic glutamic acids and checked for

their capacity to mediate antiviral signaling in response to 5'ppp-dsRNA (main figure 7A). **(A)** As a control, the same residues (indicated) were mutated into alanines and checked upon transfection of 293T cells. Mutation of S8, T667 and T667+T671 did not impact the functionality of RIG-I. Replacing all identified phosphosites or all sites of cluster I (see figure 6F) by alanines abrogated signaling. Results of one representative out of three experiments are given. **(B,C)** A549^{RIG-I KO} cells were reconstituted with empty vector or the indicated wildtype or phosphomimetic variants of RIG-I and infected with FLUAV at MOI=0.01 (analogous to main figure 7F) **(B)** or left uninfected **(C)**. FLUAV NP protein as a marker for infection and IFIT1 as a marker for active antiviral signaling were stained and analyzed in flow cytometry.

<i>Name</i>	<i>Tag</i>	<i>Promoter</i>	<i>ORF library</i>	<i>(Sub-) Cloned</i>	<i>Gift from</i>
<i>ALPK1</i>	Flag	CMV			Dr. Alexey Ryazanov, Robert wood Johnson Medical School New Jersey
<i>BMX</i>	HA	CMV			Prof. Olli Silvennoinen, university of Tampere
<i>CDC42SE2</i>	V5	CMV		X	
<i>CDKL3</i>	V5	CMV	X		
<i>DAPK1</i>	Flag	CMV		X	Prof. A. Kimchi Weizmann Institute of Science
<i>DDR1</i>	V5	CMV		XX	Prof. Friedemann Kiefer Max-Planck-Institute for Molecular Biomedicine
<i>DGKD</i>	3xFlag	CMV			Dr. Fumio Sakane Chiba University Japan
<i>EPHA1</i>	V5	CMV	X		
<i>FASTK</i>	V5	CMV	X		
<i>GK2</i>	V5	CMV	X		
<i>IRAK1</i>	V5	CMV			Prof. Alexander Weber, University of Tübingen
<i>IRAK2</i>	V5	CMV			Prof. Alexander Weber, University of Tübingen
<i>IRAK4</i>	V5	CMV			Prof. Alexander Weber, University of Tübingen
<i>ITPKC</i>	GFP	CMV			Dr. Marcus Nalaskowski, Universitätsklinikum Hamburg-Eppendorf
<i>MATK</i>	V5	CMV	X		
<i>MARK2</i>	V5	CMV	X		
<i>RIOK3</i>	V5	CMV		X	
<i>RIPK4</i>	V5	CMV	X		
<i>RPS6KA2</i>	V5	CMV	X		
<i>SKP2</i>	V5	CMV		X	
<i>SH3BP4</i>	GFP	CMV			Prof. Pier Paolo Di Fiore, IFOM-IEO Campus
<i>RIG-I</i>	HA Myc Flag		x		
<i>IFIT1 promoter lucif. reporter</i>					pGL3B/561, kind gift of Dr. Ganes Sen (Cleveland)
<i>NFκB luciferase reporter</i>					pGL4.32[luc2P/NFκB-RE/Hygro] (Promega)

Table S1. Overexpression Constructs, Related to STAR Methods. Table lists expression constructs for the indicated transgenes (*name*) with their respective tags and promoters. The cDNAs were either taken from the ORFeome library (“X” in column “ORF library”), were kind donations of the indicated colleagues (“*gift from*”) or were cloned by RT-PCR from Huh7 mRNA (“X” in column “(Sub-)cloned”). DDR1 was subcloned from a provided plasmid (“XX” in column “(Sub-)cloned”).

<i>Name</i>	<i>sequence</i>	<i>provider</i>
<i>Hs_ALPK3_8</i>	TCGGTGCACCATCCACAATGA	Qiagen
<i>Hs_BMX_5</i>	CCCAATATGACAACGAATCAA	Qiagen
<i>Hs_CDC42SE2_2</i>	AAGGGAGGTTATGGAGGTGGA	Qiagen
<i>Hs_CDKL3_5</i>	TGGGCAGATAGTGGCCATTAA	Qiagen
<i>Hs_DAPK1_5</i>	AAGCATGTAATGTTAATGTTA	Qiagen
<i>Hs_DDR1_10</i>	CAGGAATGATTTCTGAAAGA	Qiagen
<i>Hs_DGKD_5</i>	CAGCAGATTCTCTTCTATGAA	Qiagen
<i>Hs_EPHA2_5</i>	AAGGAAGTGGTACTGCTGGAC	Qiagen
<i>Hs_FASTK_8</i>	CAGCAGCAAGgTGGTACAGAA	Qiagen
<i>Hs_GK2_5</i>	TAGTAACTTCGTCAAGTCTAA	Qiagen
<i>Hs_IRAK1_5</i>	CCGGGCAATTCAGTTTCTACA	Qiagen
<i>Hs_IRAK2_5</i>	CAGCAACGTCAAGAGCTCTAA	Qiagen
<i>Hs_IRAK3_6</i>	GGAUGUUCGUCAUUAUGAATT	Qiagen
<i>Hs_IRAK4_6</i>	ATCCTATTAGTCATATATTTA	Qiagen
<i>Hs_ITPKC_5</i>	CAGAAGGAGCCTGTCCCTCAA	Qiagen
<i>Hs_MARK2_6</i>	CACCTCTAATTCTTACTCTAA	Qiagen
<i>Hs_MATK_9</i>	ACGGATTCTAAGGACTCTAAA	Qiagen
<i>Hs_RIPK4_5</i>	AAGCCTGATGACGAAGTGAAA	Qiagen
<i>Hs_RPS6KA2_9</i>	CCGAGTGAGATCGAAGATGGA	Qiagen
<i>Hs_SH3BP4_5</i>	CACCACGAATAGCACTGGCAA	Qiagen
<i>Hs_SKP2_5</i>	AAGTGATAGTGTCATGCTAAA	Qiagen
<i>All star negative</i>	not revealed by the company (SI03650318)	Qiagen
<i>RIG-I</i>	AACGUUUACAACCAGAAUUUA	MWG
<i>MAVS</i>	CCCACAGGGUCAGUUGUAU	MWG
<i>Mouse_DAPK1_1</i>	AAGGATTGACGTCCAGGATAA (Mm_Dapk1_2)	Qiagen
<i>Mouse_DAPK1_2</i>	AAGCCTAAAGACCACCCAACAA (Mm_Dapk1_4)	Qiagen
<i>DAPK1</i>	AAGCATGTAATGTTAATGTTA (Hs_DAPK1_5)	Qiagen
<i>DAPK1_2</i>	not revealed by the company (SIHK0538)	Sigma-Aldrich
<i>DAPK1_3</i>	not revealed by the company (SIHK0539)	Sigma-Aldrich

Table S2. Sequence or Ordering Information of siRNAs, Related to STAR Methods. siRNAs were ordered from commercial vendors. Where sequence information was not revealed, the table lists ordering numbers. Names of Qiagen siRNAs starting with “Hs_” are also direct product identifiers.

<i>Target Gene</i>	<i>F Primer</i>	<i>R Primer</i>
<i>GAPDH</i>	GAAGGTGAAGGTCGGAGTC	GAAGATGGTGATGGGATTTTC
<i>IFIT1</i>	GAAGCAGGCAATCACAGAAA	TGAAACCGACCATAGTGGAA
<i>IFNB</i>	CGCCGCATTGACCATCTA	GACATTAGCCAGGAGGTTCTC
<i>dsRNA</i>	CTTCTCTTGTTGGGCCAC	TCCTGGCCTGTGAGTTCTTG

Table S3. Primer Sequences of qRT-PCR Primers, Related to STAR Methods. Table lists sequences for forward (F) and reverse (R) primers used for quantitative RT-PCR.

Name	sequence
RIG-I cloning	
S8E	F: ggggacaagttgtacaaaaaagcaggcttcatgaccaccgagcagcgacgcgagctgcaagcctc R: ggggaccactttgtacaagaaagctgggtctcatttggacatttctgctggatc
S8A	F: ggggacaagttgtacaaaaaagcaggcttcatgaccaccgagcagcgacgcgagctgcaagcctc R: ggggaccactttgtacaagaaagctgggtctcatttggacatttctgctggatc
cluster I to E	F: ggattgaaggaaatcctaaactcgagtttctaaaacctggcatattgactggacgtggcaaagaaatcaga acgaaggaatggagctcccggcacagaagtgtatattgg R: aatfttttaaagcgctccacaagtgc
cluster I to A	F: ggattgaaggaaatcctaaactcgcttttctaaaacctggcatattgactggacgtggcaaagcaaatcagaa cgcaggaatggcctcccggcacagaagtgtatattgg R: aatfttttaaagcgctccacaagtgc
cluster II to E	F: tgatgaatgacgagattttacgccttcaggaatgggacgaagcagtatttag R: tttttctttgtacatgtttattgttc
cluster II to A	F: tgatgaatgacgctattttacgccttcaggcatgggacgaagcagtatttag R: tttttctttgtacatgtttattgttc
T667E + T671E	F: catattgactggacgtggcaaagaaaatcagaacgaaggaatgaccctcccggcac R: ccaggtttagaaaactgag
T667A + T671A	F: catattgactggacgtggcaaagcaaatcagaacgcaggaatgaccctcccggcac R: ccaggtttagaaaactgag
T667E	F: catattgactggacgtggcaaagagaatcagaacacaggaatgaccctc R: ccaggtttagaaaactgag
T667A	F: catattgactggacgtggcaaagcgaatcagaacacaggaatgaccctc R: ccaggtttagaaaactgag
T671E	F: catattgactggacgtggcaaaacaaatcagaacgaggaatgaccctc R: ccaggtttagaaaactgag
T671A	F: catattgactggacgtggcaaaacaaatcagaacgcgggaatgaccctc R: ccaggtttagaaaactgag
DAPK1 cloning	
full-length DAPK1	F: ggggacaagttgtacaaaaaagcaggcttcatgaccgtgttcaggcagg R: ggggaccactttgtacaagaaagctgggtctcaccgggatacaacagagc
kinase domain (KD)	F: ggggacaagttgtacaaaaaagcaggcttctacgacaccggcgaggaactgg R: ggggaccactttgtacaagaaagctgggtctcagatccagggatgctgcaaac
KD + CaM	F: ggggacaagttgtacaaaaaagcaggcttctacgacaccggcgaggaactgg R: ggggaccactttgtacaagaaagctgggtctcaatcgcttctggcaacactc
Δ DD	F: ctgaacctcctcactcggaggtctgtgtcaaaatcaacctgg R: ccaggttgattttgaacacagacctcagtgaggaggtcag
Δ Ank + ROC + COR	F: gatgtaaccaaccaacaagcaggtccgcggcctggagacgg R: ccgtctccaggcccgacactgctgtgggttggttaacatc
Δ ROC domain	F: gatgggagccagcgtgaggcgaagctgaagaaccactccaag R: ctggagtggttctcagcttcgctcaacgctggctcccatc
Δ CaM	F: gaagagaatgacaattgatactctggatgaggaag R: ctctcatccagagtatcaattgtcattctctc
KD + CaM + Ank	F: ggggacaagttgtacaaaaaagcaggcttcatgaccgtgttcaggcagg R: ggggaccactttgtacaagaaagctgggtctcagcctcaacgctggctcccatcag
Ank domain	F: ggggacaagttgtacaaaaaagcaggcttcatgatactctggatgaggaagactcctttg R: ggggaccactttgtacaagaaagctgggtctcagcctcaacgctggctcccatcagac
KD CaM Ank K42A	F: gcctccagatgccgcccattcatcaagaaaag R: ctttcttgatgaatgcccggcactactggagggc
KD CaM Ank S308D	F: gaaaaaatggaacaagcgttcgcttgatatac R: gatataagcgaacgtctgttccatttttc
KD CaM Ank S308A	F: gaaaaaatggaacaagcgttcgcttgatatac R: gatataagcgaacggctgttccatttttc
KD CaM Ank Δ 1-73	F: ggggacaagttgtacaaaaaagcaggcttcatgccaatgtcatcacctgcacg R: ggggaccactttgtacaagaaagctgggtctcagcctcaacgctggctcccatcag

Table S4. Primer Sequences of Cloning Primers, Related to STAR Methods. The listed forward (F) and reverse (R) primers were used to generate the indicated RIG-I or DAPK1 constructs by standard cloning procedures (see STAR Methods).

Supplemental data file 1 - Screening results.xlsx, Related to Figure 1. The data file contains two tabs, one holding the data (p-values and enrichment scores) of the primary screen, one holding the data for all validation screens. The latter tab furthermore contains Boolean columns representing the hit calling criteria described in the STAR Methods.

Supplemental data file 2 - Functional annotation clustering.xls, Related to Figure 1. This data table contains the results of a DAVID functional annotation clustering, using DAVID version 6.8 (beta). For the analysis, all primary hit genes were included (i.e. each gene that had at least one siRNA with a p-value of <0.05; in total 102 DAVID IDs). All genes represented in the siRNA library were defined as the background for the analysis (720 unique GeneIDs, see tab "Primary screen genes"). For selected functional annotation clusters, information at the single gene level are given in separate tabs.

Supplemental data file 3 - PPI and virus screens.xlsx, Related to Figure 1. This data file contains the results of the protein-protein-interaction (PPI) analyses performed on the list of screening hits, as well as overlap analyses with previously published virus replication screens. For more information, refer to the STAR Methods section.